MASTER THESIS FOR THE DEGREE MASTER OF PHARMACY

LIPOSOMES AS DRUG DELIVERY SYSTEM IN MITOCHONDRIAL TARGETING

BY

ELSE MARI ØDEGAARD-JENSEN

2012

External Supervisor

Prof. Dr. Regine Süss

Pharmaceutical Technology
and Biopharmacy
Institute of Pharmaceutical Sciences
Faculty of Chemistry, Pharmacy
and Earth Sciences
University of Freiburg

Internal Supervisor

Prof. Dr. Nataša Škalko-Basnet

Drug Transport and Delivery
Research Group
Department of Pharmacy
Faculty of Health Sciences
University of Tromsø

Acknowledgement

The present work was carried out at Pharmaceutical Technology and Biopharmacy, Institute of Pharmaceutical Sciences, University of Freiburg, Germany from September 2011 to March 2012.

First I want to thank Prof. Dr. Regine Süss for letting me join the working group in Freiburg. It was six months with lots of learning and lots of fun.

Ying Zhou, I really appreciated working with you. Congratulation with your PhD and I wish you good luck with your baby.

I want to thank Birgit Erhard for all possible help in the lab. I also greatly appreciate the work of Nicole Specht who performed the Bartlett assay, Sabine Barnert who performed the Cryo-Transmissions-Electron microscopic studies and Irmgard Ohlhoff who ordered lipids for me.

To the rest of the working groups of Prof. Dr. Shubert and Prof. Dr. Süss, thank you so much for accepting me as a part of the group. *Ich hatte viel spass euch in Cafe Knastblick anzuhören.*

I really appreciate the endless help from Prof. Dr. Nataša Škalko-Basnet during writing of the thesis. Without your help, I would not have managed to finish.

I also want to thank my brother Arvid who is able to help, even from a different academic field.

Last, but not least, I want to thank the rest of my family and my friends for keeping my motivation up to continue working, giving me 5 wonderful years in Tromsø.

Else Mari Ødegaard-Jensen
Tromsø, May 2012

Table of contents

List of figures

List of tables

Abstract

The mitochondrion is a subcellular organelle with major functions related to energy production and control of apoptosis. The presence of mitochondria as a subcellular organelle has been known for more than one and a half century. However, only the last decades' research has discovered their role in ageing and disease pathology, which have led to increasing interest in mitochondria as target for drug delivery. For a long time the mitochondria were thought to be static organelles, however, it was then discovered that they continuously fused together forming tubular networks followed by fission back into single organelles.

The aim of the work was to evaluate whether liposomes could be recognized as artificial mitochondria and thereby be included in the fusion-fission cycle.

Liposomes were prepared with different lipid compositions mimicking the composition of the outer mitochondrial membrane. A lipophilic fluorescent dye was incorporated in liposomes to evaluate their ability to fuse with isolated mitochondria.

Based on the fusion experiments, it was confirmed that the level of fusion was altered in respect to the different lipid compositions.

Key words: mitochondria, targeting, fusion-fission cycle, liposomes, drug delivery

List of abbreviations

aCoA	Acetyl coenzyme A
AD	Alzheimer's disease
ADP	Adenosine diphosphate
ATP	Adenosine triphosphate
Bcl-2	B-cell lymphoma-2
BSA	Bovine serum albumin
CCCP	Carbonyl cyanide 3-chlorophenylhydrazone
CL	Cardiolipin
CoA	Coenzyme A
CoQ	Coenzyme Q
Cyt c	Cytochrome *c*
DM	Diabetes mellitus
Drp-1	Dynaminn-related protein 1
ETC	Electron transport chain
$FADH_2$	Fully reduced flavin adenine dinucleotide
Fis1	Fission protein 1
GDP	Guanosine 5'-diphosphate
GPL	Glycerophospholipids
IB	Isolation buffer
IMM	Inner mitochondria membrane
IMS	Intermembrane space
Mfn	Mitofusin
MM	Mitochondria matrix
MPS	Mononuclear phagocyte system
mtDNA	Mitochondrial DNA

OMM	Outer mitochondrial membrane
OPA1	Optic atrophy protein 1
NAD^+	Nicotinamide adenine dinucleotide
NADH	Reduced nicotinamide adenine dinucleotide
OMM	Outer mitochondria membrane
PC	Phosphatidylcholine
PD	Parkinson’s disease
PE	Phosphatidylethanolamine
PG	Phosphatidylglycerol
PI	Phosphatidylinositol
R18	Octadecyl rhodamine B chloride
R123	Rhodamine 123
ROS	Reactive oxygen species
TCA	Tricarboxylic acid
TPP	Tirphenylphosphonium

1 General introduction

Mitochondria are a subcellular organelles thought to rise from the endosymbiosis theory (Nunnari and Suomalainen, 2012). They have a distinct structure consisting of two membranes which is important in one of their major functions; producing the energy, in form of adenosine triphosphate (ATP), the cell need to carry on its function (Kowald and Kirkwood, 2011a). They are also important regarding their role in controlling apoptosis and mitochondrial dysfunctions shows to be the cause of an increasing number of human disorders (Nunnari and Suomalainen, 2012).

It was earlier thought that mitochondria were static organelles, but they were later shown to be quiet dynamic with a constant on-going cycle of alternating fusion and fission (Kowald and Kirkwood, 2011a). Evidence shows that alternating fusion and fission is necessary as a quality control in order to repair or destroy damaged organelles (Otera and Mihara, 2012). The accurate delivery of proteins and lipids due to different needs regarding intracellular location (Otera and Mihara, 2012) and correct distribution in cell division (Zungu et al., 2011) is also managed by this cycle.

Liposomes are a novel form of drug delivery systems, although they have been known for several decades (Brandl, 2001). Different lipids are distributed differently in biological membranes (Welti and Glaser, 1994) and might therefor have distinct roles in membrane function.

2 Introduction

2.1 Mitochondria

2.1.1 Structure and characteristics

The mitochondrion is an approximately 2 μm long eukaryotic subcellular organelle which is thought to originate from the endosymbiosis theory. This theory states that an oxygen consuming bacterium was engulfed by a eukaryotic ancestor cell (Nunnari and Suomalainen, 2012). Since both had benefits from the others function they stayed together in a symbiotic relationship (Jianping, 2010).

There are two main factors, from a structural point of view, which differs the mitochondria from the other organelles – the double membrane, as illustrated in Figure 1, and the presence of mitochondrial DNA (mtDNA).

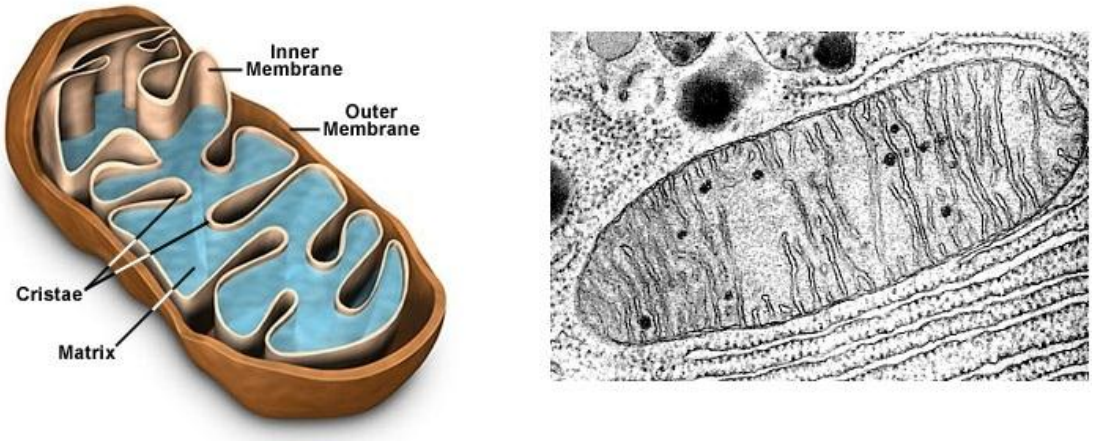

Figure 1 Structure (left) (MolecularExpressions™, 2004) **and micrograph (right)** (Kimball'sBiologyPages, 2012) **of mitochondria**

The double membrane consists of the outer mitochondrial membrane (OMM) and the inner mitochondrial membrane (IMM), both being phospholipid bilayers but with different composition, divided by an intermembrane space (IMS). The OMM consists of porins which allows ions and small molecules from cytosol to freely move into IMS. The IMS contain important ions, molecules and proteins for the mitochondrion to maintain normal functions. This includes protons responsible for the membrane potential and key participants in ATP

production and cytochrome *c* (cyt c) which serves as an inducing agent in apoptosis. The IMM works as a barrier for most solutes to keep the IMM and the mitochondrial matrix (MM) as separate compartments. It also serves as the site of action for the electron transport chain (ETC) and the energy production in form of ATP.

The mitochondria was observed as early as in the 1850s, but it took more than a century before its genome was discovered in the 1960s (Zick et al., 2009). According to the endosymbiosis theory, when the bacterium entered the cell it brought its own genome. During evolution most of the protein coding has been transferred to the nucleus**,** but there is still some intact genome left in the mitochondrion which codes for 13 proteins necessary in the respiratory complexes and RNAs necessary for the translocation (Taylor and Turnbull, 2005; Nunnari and Suomalainen, 2012).

One of the most important tasks of the mitochondria is the production of ATP which counts for 90% of the energy needed in the cells and tissues (Kowald and Kirkwood, 2011a; Marchi et al., 2012). The mitochondria also function as a control point for the onset of apoptosis and have been shown to play a role in aging and different human disorders (Zick et al., 2009).

The location of the mitochondria correspond to the energy consumption of the cell where the cells with the highest need of energy have the highest number of mitochondria and they tend to have intracellular accumulate where the energy is needed.

2.1.2 Metabolic functions

The mitochondria are often referred to as the "powerhouse" of the cell. However, there are also other important activities located in different parts of the mitochondria, for example apoptosis (discussed below) and signalling (Zhang and Chan, 2007).

In this section the focus will be on the mitochondrial metabolic pathway leading to ATP synthesis, starting with β-oxidation of fatty acids whose product, acetyl coenzyme A (aCoA), is a substrate in the tricarboxylic acid (TCA) cycle taking place in MM. Reduced nicotinamide adenine dinucleotide (NADH), produced in TCA cycle, drives the electron transport chain (ETC) whose resulting proton gradient across the inner membrane is necessary for the synthesis of ATP.

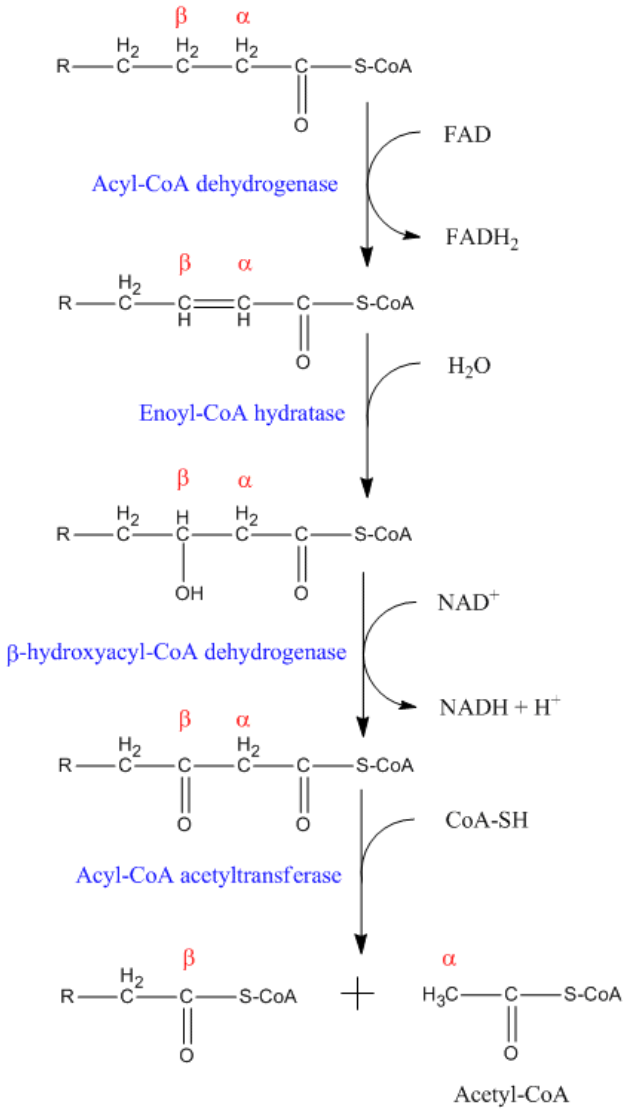

Figure 2 Chemical pathway in β-oxidation of fatty acids (Nelson and Cox, 2008)

About 50-75% of fatty acid β-oxidation in animals occurs in the mitochondria, which includes fatty acids with a chain length shorter than 16 carbon atoms (Becker et al., 2006a). Longer acyl chains are first shortened in peroxisomes before transported to mitochondria for complete degradation. Even numbered acyl chains with number of C = n will, after complete β-oxidation, result in n/2 aCoA and (n/2)-1 fully reduced flavin adenine dinucleotide ($FADH_2$) and NADH as illustrated in Figure 2.

ACoA can also be obtained from glycolysis where the primary end product is pyruvate. Through the IMM, the pyruvate carrier transports pyruvate into the MM where pyruvate dehydrogenase oxidizes pyruvate to aCoA with the help of coenzyme A and (nicotinamide adenine dinucleotide) NAD^+ resulting in CO_2 and NADH as by-products.

To enter the TCA cycle aCoA condensation with oxaloacetate to generate citrate is catalysed by citrate synthase, as shown in Figure 3. One water molecule is consumed as the coenzyme A (CoA) and one proton is released.

Via the intermediate *cis*-aconitate, citrate is transformed to isocitrate by the bidirectional aconitase. The next step is also via an intermediate, the unstable oxalosuccinate is formed by oxidation catalyzed by isocitrate dehydrogenase with help of NAD^+ forming NADH followed by decarboxylation into α-ketoglutarate with release of CO_2. A further oxidation catalyzed by α-ketoglutarate dehydrogenase and inclusion of NAD^+ and CoA results in succinyl CoA and release of CO_2 and the generation of another NADH. Conversion of succinyl CoA to succinate is catalyzed by the bidirectional succinyl-CoA synthetase and the CoA is released again. In the same step an inorganic phosphate is condensed with guanosine 5'-diphosphate (GDP) forming guanosine 5'-triphosphate (GTP) which can return to GDP by giving one phosphate to adenosine diphosphate (ADP) resulting in formation of one ATP.

Succinate dehydrogenase catalyzes the oxidation of succinate to fumarate and one $FADH_2$ is formed from flavin adenine dinucleotide (FAD). Fumarate hydratase then consumes one water molecule in order to hydrate fumarate to malate. Further oxidation by malate dehydrogenase results in oxaloacetate with additional formation of NADH from NAD^+ and release of a proton. The cycle can then start over again with inclusion of a new aCoA.

To summarize, the TCA cycle produce three NADH, two protons, one $FADH_2$ and one ATP that can be utilized later.

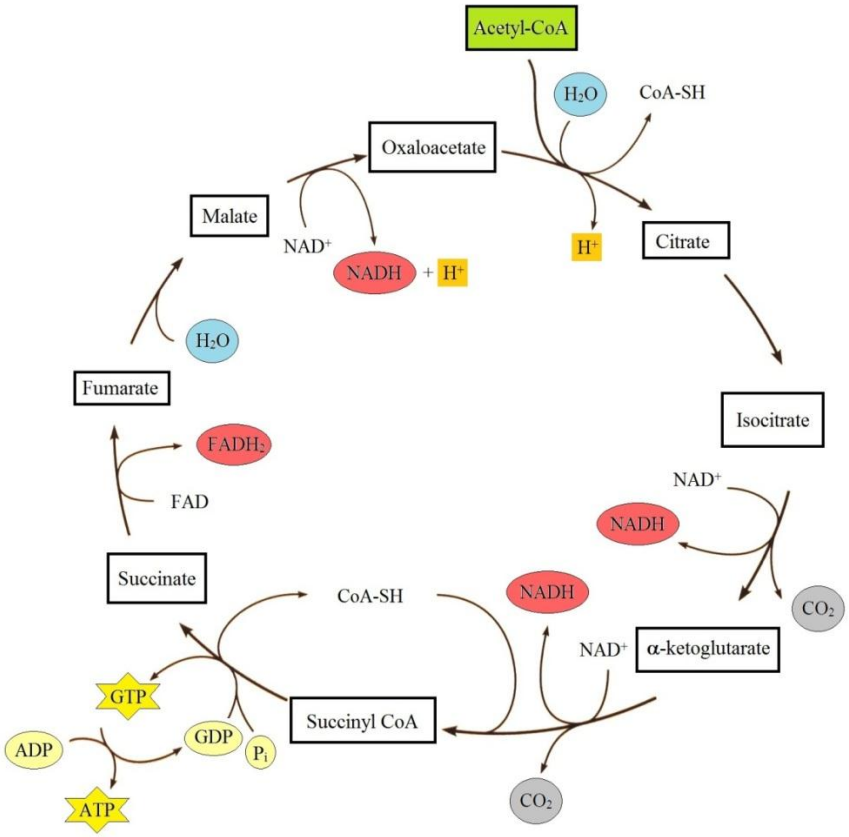

Figure 3 Tricarboxylic acid cycle (Becker et al., 2006b)

The ETC, also called respiratory chain, is a set of complexes gathered in the IMM. The bottom line of the electron transport is the transport of electrons from coenzymes like NADH to molecular oxygen, and the function of the complexes is to link this transfer of electrons with the pumping of protons from MM to IMS (Weiss et al., 1991). However, it is not as straight forward as indicated in Figure 4.

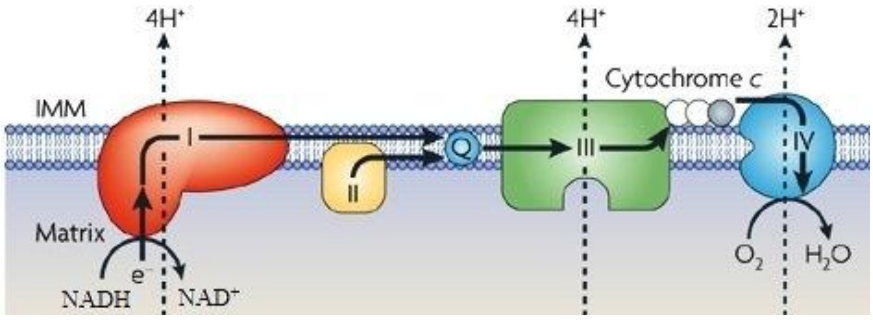

Figure 4 Basic schematic steps in the electron transport chain (Ow et al., 2008)

Complex I, also called NADH-coenzyme Q (CoQ) oxidoreductase, transfer two electrons from NADH to CoQ resulting in binding of two protons. Each pair of electrons that passes the complex results in pumping of four protons across the membrane directly from MM.

Complex II, also called succinate-CoQ oxidoreductase, transfers two electrons to CoQ from $FADH_2$. No proton pumping is coupled with this electron transfer.

Complex III, also called CoQ-cytochrome c (cyt c) oxidoreductase, transfers the electrons from CoQ to cyt c. Each pair of electrons that passes the complex results in pumping of four protons across the membrane, two which comes from CoQ and two directly from MM.

Complex IV, also called cyt c oxidase, transfers the electrons from cyt c to oxygen. Each pair of electrons entering the complex results in removal of four protons from MM. Two of those protons are used to make a water molecule together with one half of an O_2 molecule. The two remaining protons are just pumped across the membrane.

The ATP synthase, also called complex V in ETC, is located in the IMM where it uses the protons pumped out into the IMS by the ETC to drive the condensation of ADP to ATP, as illustrated in Figure 5. For each proton entering the MM though the IMM traversing part of the protein, one ADP and inorganic phosphate group is docked into binding sites, one ADP and inorganic phosphate group is condensed to ATP in another binding site and one ATP is released from a third binding site. This means that three protons are necessary to pass through the protein in order to complete one condensation process.

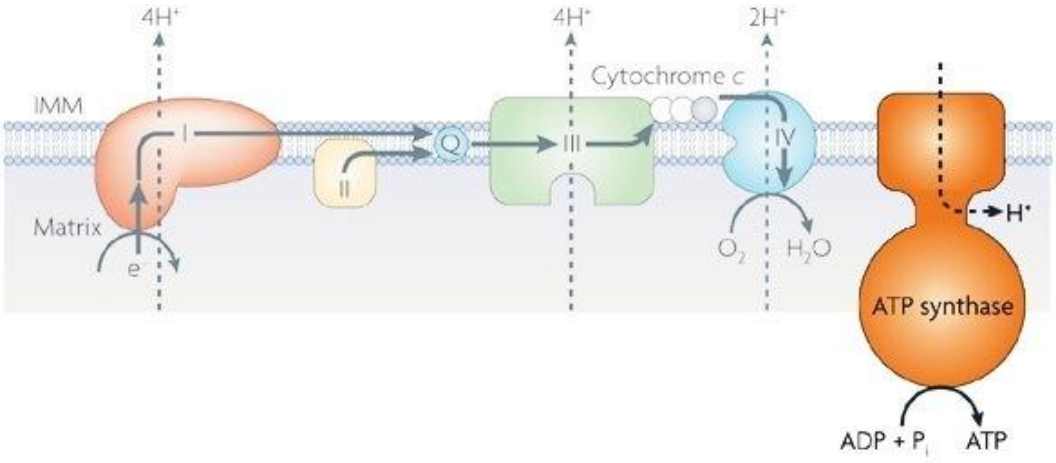

Figure 5 ATP production in inner mitochondrial membrane and coupling with electron transport chain (Ow et al., 2008)

2.1.3 Apoptosis

Apoptosis is programmed killing of cells in a way that is as gentle as possible to the surrounding cells (Indran et al., 2011) and it is essential both in organ development and in life as general (Desagher and Martinou, 2000). There are 2 main initial routes of apoptosis, as shown in Figure 6, one being activation due to cell death signal, left side, and the other being activation by removal of survival factors, right side. There have been discovered cross talking between the routs (Wang and Youle, 2009), but it is the latter one will be in focus here.

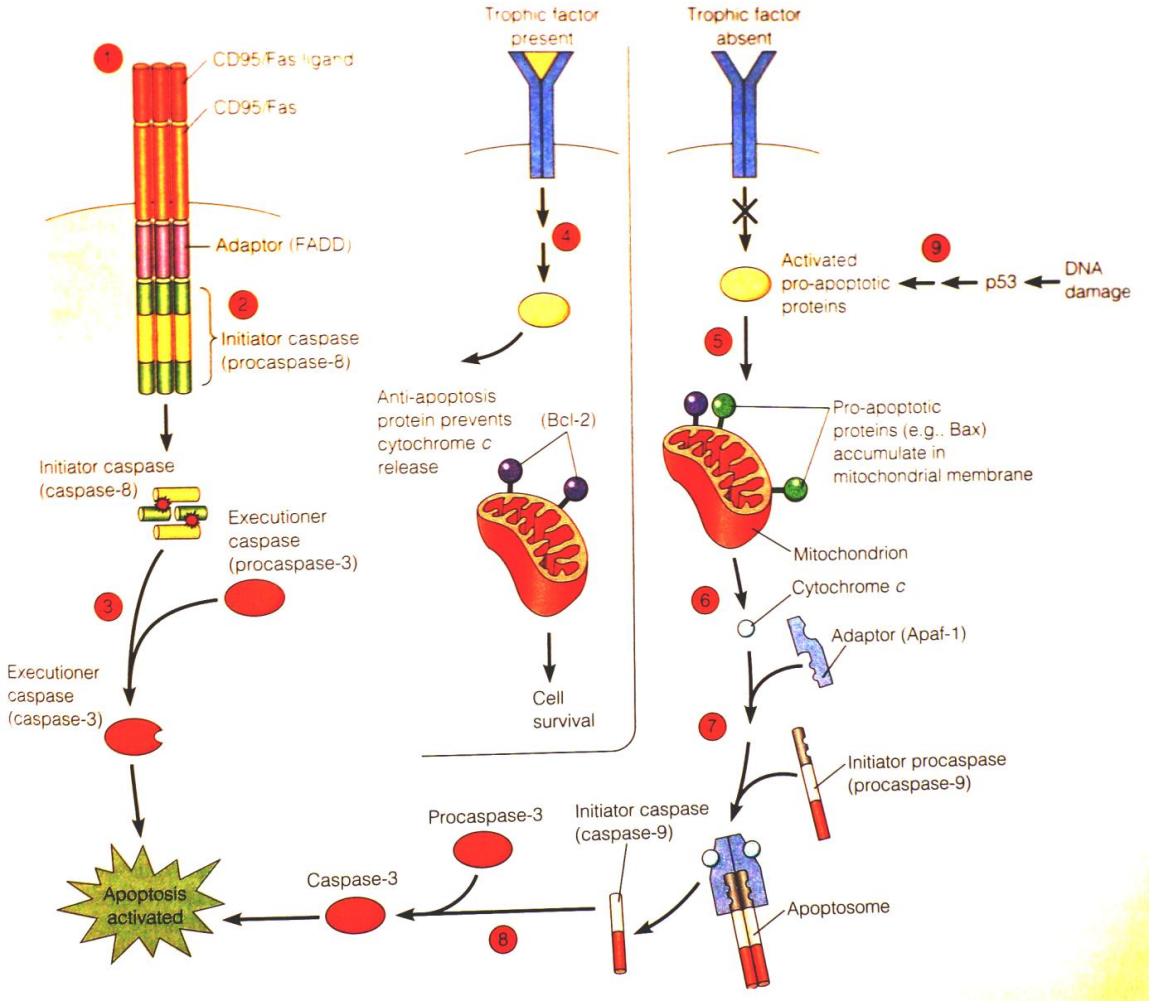

Figure 6 Schematic steps in apoptosis (Becker et al., 2006c)

Survival, or trophic, factors keeps the cells alive. This is maintained by inhibiting activation of pro-apoptotic proteins, for example Bcl-2-associated X protein (Bax). In the absence of this factors, pro-apoptotic proteins will be activated and then accumulate in the OMM leading to release of IMS proteins like cyt c (Wang and Youle, 2009). However, there is always a

balance in the OMM between anti-apoptotic, for example B-cell lymphoma-2 (Bcl-2), and pro-apoptotic factors. The main function of anti-apoptotic factors has been shown to be preventing of cyt c release (Desagher and Martinou, 2000), but when the balance shifts towards pro-apoptotic factors the activation of apoptosis will start.

The cytosolic cyt c binds to an adaptor protein, apoptosis protease-activating factor 1 (Apaf-1), with help of ATP, making apoptosomes, and this complex will then activate the first caspase in the cascade; one caspase activates the next ending in activation of apoptotic morphological changes (Schug and Gottlieb, 2009). Cyt c release have been stated as a "point of no return" in apoptosis (Gogvadze et al., 2009), however, if the caspase activity is blocked it has been shown that the on-going process towards apoptosis will stop, which indicates how finely tuned and tightly controlled this process is (Wang and Youle, 2009).

2.1.4 Fusion-fission cycle

Fusion and fission are very common in the body and include exo- and endocytosis, fertilization and cell division. Mitochondrial fusion and fission are constant on-going processes (Westermann, 2010), as illustrated in Figure 7. However, the exact mechanism and the function of the alternating fusion and fission of mitochondria are still not totally clear. The main problem seems to be how the fusion of the outer and inner membranes is coordinated relative to each other.

Experiments have shown that mitofusins 1 and 2 (Mfn1 and Mfn2) in the OMM and optic atrophy protein 1 (OPA1) in the IMM are essential in the mitochondrial fusion process (Westermann, 2010; Zungu et al., 2011). Mfn1 tends to facilitate the membrane tethering of the fusing mitochondria, Mfn2 the OMMs fusion and OPA1 the fusion of the IMMs (Zungu et al., 2011).

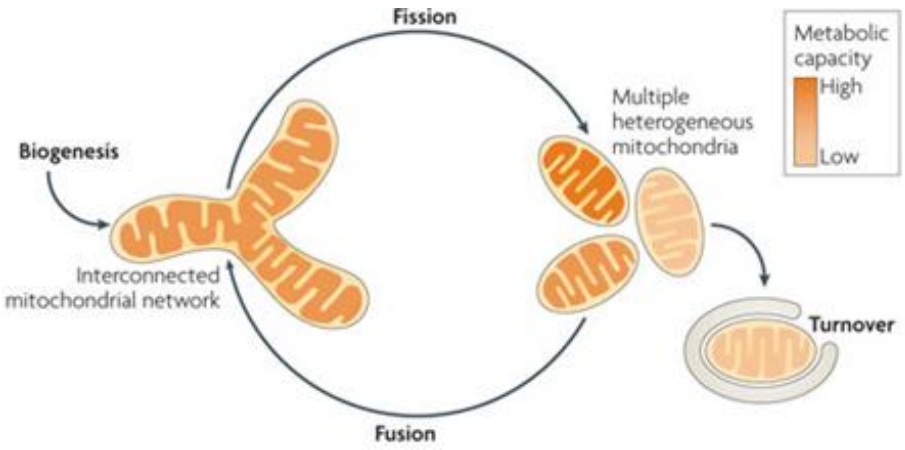

Figure 7 Overview of mitochondrial fusion-fission cycle (Westermann, 2010)

Since mitochondria are unequally distributed throughout the cell their need for proteins varies due to different metabolic activity. Fusion might then solve the problem regarding accurate delivery to each organelle (Kowald and Kirkwood, 2011b). It has been shown that fusion depend on functional membrane potential and mitochondria with a diminished membrane potential will thereby be excluded (Twig et al., 2008), however, it might also play a role in repair of slightly damaged mitochondria (Zungu et al., 2011). Pro-apoptotic factors are thought to regulate mitofusin function and thereby regulate fusion which leads to the assumption that fusion protect against apoptosis. (Zhang and Chan, 2007).

The cytosolic dynamin-related protein-1 (Drp-1) and fission protein 1 (Fis1) in the OMM are shown to be essential in the mitochondrial fission process (Zungu et al., 2011). Drp-1 lack docking protein in the membrane and therefor use Fis-1 as an adaptor protein to initiate fission, then dislocates back to cytosol after completed fission (Zungu et al., 2011).

Fission is an important quality control where damaged mitochondria can be removed and the functional mitochondria can be distributed in the cell according to the local need of ATP (Otera and Mihara, 2012). It has also been observed increased fission rate in cells committed to apoptosis (Otera and Mihara, 2012) which might correlate to the fragmentation during apoptosis. Fission is also important in cell division regarding correct distribution of mitochondria and mtDNA to each daughter cell (Zungu et al., 2011).

2.1.5 Role in different diseases

In the 1990s, evidences that mitochondrial dysfunction can cause diseases started to appear (Boddapati et al., 2008) and the number of disorders are continuously increasing (Nunnari and Suomalainen, 2012). Since mitochondria are present throughout the body, the impaired mitochondrial function can cause defects in any organ (Petruzzella et al., 2012). When dysfunctional mitochondria accumulate in the cell it will impair cellular function and might lead to several chronic diseases (Twig et al., 2008). These disorders are in basic thought to be unrelated, but evidence suggests that reactive oxygen species (ROS) is a common factor in the pathophysiology (Pieczenik and Neustadt, 2007).

Most of the mitochondria in the human embryo come from the egg – the contribution from the sperm is almost negligible (Sato and Sato, 2012). As a result of this almost all mutations, and thereby diseases, are inherited from the mother.

Diabetes mellitus (DM) is a metabolic disorder divided in two types. Type 1 is characterized by total absence of insulin production as a result of pancreatic β-cell destruction while type 2 is characterized by insulin resistance and decreased insulin secretion (Correia et al., 2012). It has been thought that intracellular hyperglycemia can result in increased production of ROS and that the following oxidative stress experienced by the cell can contribute to the development of DM (Naudi et al., 2012). Hyperglycemia is also responsible for a relative decrease of antioxidants, due to increased glucose conversion, leading to increased sensitivity to oxidative stress (Rolo and Palmeira, 2006). There are two ways that can link mitochondria to the development of DM, the first being inheritance of mtDNA mutation (Enns, 2003) and the second being the fact that mitochondria are the main source of ROS with a majority generated from ETC (Rolo and Palmeira, 2006).

Alzheimer's disease (AD) is a common form of dementia with progressive increase in severity (Correia et al., 2012). Damages due to oxidative stress has been observed in AD patients (Enns, 2003; Moreira et al., 2010) and appears to be a key factor in both development and progression of the disease (Reddy, 2008). Together with a higher risk of AD in patients with DM it is suggested that the disorders have some common pathology (Correia et al., 2012).

Parkinson's disease (PD) is a common neurodegenerative disease characterized by muscle rigidity and tremor (Enns, 2003) which is caused by degeneration of dopaminergic neurons in substantia nigra (Reddy, 2008). PD has a complex pathophysiology, but oxidative damage and reduced function of ETC, especially complex I, have been reported in PD (Enns, 2003; Reddy, 2008; Cali et al., 2011) and mtDNA mutations have been observed as possible and partly explanations for ECT dysfunction (Reddy, 2008; Cali et al., 2011).

Cancer cells, whose natural onset of apoptosis is silenced, have a high rate of cell division (Gogvadze et al., 2009). Healthy cells get most of their ATP from ETC in mitochondria while cancer cells instead use up-regulated glycolysis as the main energy source (Indran et al., 2011). There have been shown a proportional relationship between increased rely on glycolysis and aggressiveness of tumor cells (Gogvadze et al., 2009). ROS have a dual role regarding cancer since oxidative stress can lead to mutations or damages resulting in tumor development and the elevated level in cancer cells are vital to cell survival, but in excessive amounts it will lead to cell death (Azad et al., 2009). Both physiological alteration, like fewer mitochondria per cell, with smaller size and increased membrane potential (Indran et al., 2011), and down-regulated metabolic activity (Gogvadze et al., 2009) might explain the resistance towards apoptosis in cancer cells.

2.1.6 Strategies for mitochondrial targeting

The goal with targeted therapy is to selectively treat the affected organ and not interfere with healthy parts (Torchilin, 2010). This will lead to lower dose needed for the treatment and decreased incidents as well as severity of side effects.

Targeting can be divided into passive and active targeting. The former can be used in targeting tumors, for instance, where it takes advantage of the enhanced permeation and retention (EPR) effect, which relies on more leaky blood vessels relative to blood vessels in healthy tissue (Bitounis et al., 2012). When the cells or even subcellular organelles are to be reached, the therapy must be actively and selectively targeted. There are several possibilities in active targeting, but only a few are presented here. They focus on the fact that mitochondrial dysfunction can cause disorders and have therefor a common goal of inducing cell death, a concept introduced about 15 years ago (Weissig, 2011).

In cells resistant to chemotherapy the have been observed overexpression of anti-apoptotic Bcl-2 (Kang and Reynolds, 2009). Changes in sensitivity to apoptosis result in damaged cells and organelles not being removed and might lead to growth of cancer cells. The Bcl-2 would then be an appropriate target and down regulation, which would result in OMM destabilization and thereby cyt c release, can be achieved both on messenger RNA (mRNA) and protein level. A similar destabilization of OMM can be caused by inhibition of 3-hydroxy-3-methyl-guaryl (HMG) CoA reductase which results in decreased amount of cardiolipin produced that can stabilize the membrane (Gogvadze et al., 2009).

The majority of energy production in tumor cells is due to glycolysis, even though the mitochondria have a much higher output. In the glycolytic pathway one glucose and two ATP are consumed resulting in two pyruvate and four ATP. The net energy output is then two ATP in contrast to a total of 47 ATP after one complete cycle starting from production of one aCoA and ending with complex V. If glycolysis in or glucose transport into the tumor cells are depressed the ATP level will decrease. This will lead to permeabilization of OMM and thereby release of pro-apoptotic factors localized in IMS, resulting in massive cell death (Gogvadze et al., 2009).

A direct change in mitochondrial activity might be another way in which cell death can be induced. Inhibition of ETC will cause increased amount of ROS (Chen et al., 2007). In low levels, ROS act as signalling molecules which is important in cell survival, but when the levels of ROS increases it will cause cell death (Azad et al., 2009).

The approaches presented so far have been on targeting specific mitochondrial functions. Yet another way is achieving targeting based on the affinity.

Mitochondriotropic molecules are substances that, due to the membrane potential, will specifically accumulate in the mitochondria. One such example is triphenylphosphonium (TPP). By linking the TPP to a fatty acid it is possible to incorporate it in lipid membranes and thereby use it as a targeting moiety on liposome surface. Experiments have shown that TPP facilitates subcellular delivery and that incorporated drug shows increased induction of apoptosis relative to free drug or drug incorporated in non-targeted vehicle (Boddapati et al., 2008).

2.2 Liposomes

2.2.1 Liposomes as carrier systems

Liposomes are spherical lipid vesicles normally prepared from phospholipids which makes them biocompatible and biodegradable and thereby nontoxic (Lasic, 1998). They are of different size and with different number of lipid bilayers, or lamellas, and can be defined as:

> Multilamellar vesicles (MLV) are generally referred to as larger than 100 nm and can range up to several µm.
>
> Unilamellar vesicle can be divided into:
>
> - Small unilamellar vesicles (SUV) with a general size bellow 100 nm,
> - Large unilamellar vesicles (LUV) with a general size lager than 100 nm, and
> - Giant unilamellar vesicles (GUV) with a general size larger than 1 µm (Martin et al., 2006).

A great variety of components can use liposomes as carrier or protection since hydrophilic compounds can be encapsulated in the aqueous core and lipophilic and amphiphilic compounds can be incorporated in or associated with the lipid bilayer (Torchilin, 2005) as illustrated in Figure 8. This provides liposomes with a wide potential to be used in therapeutic, and cosmetic, applications.

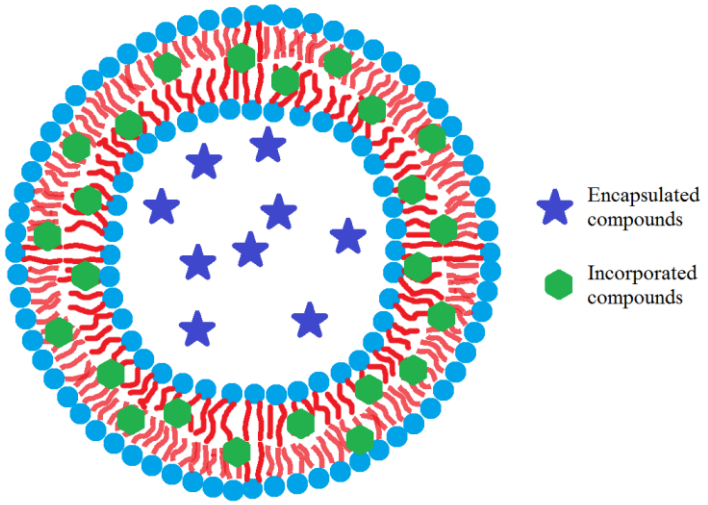

Figure 8 Schematic loaded liposome

One major drawback in liposomal pharmacotherapy is their fast clearance from blood through the mononuclear phagocyte system (MPS). To increase the circulation time, different hydrophilic polymers have been attached to the surface of the liposomes, where polyethylene glycol (PEG) is the most studied (Torchilin, 2005). It has also been reported that high-density lipoprotein (HDL) and low-density lipoprotein (LDL) reduce the liposomal stability as a result of lipid transfer, which have been solved by adding cholesterol to the liposomes (Bitounis et al., 2012).

However, major advantage with liposomal delivery over free drug delivery is the ability to target the pharmacological treatment to specific sites and thereby reducing the occurrence and severity of side effects (Lasic, 1998).

2.2.2 Lipids

Lipids can be defined both due to their biological function and their chemistry. The lipids in focus here are categorized as important for the structure of membranes and are chemically called glycerophospholipids (GPL). *Glycero-* refers to the glycerol backbone and the –*phospho-* refers to the phosphate binding the polar head group (denoted R-group) to the glycerol, as shown in Figure 9. In biological membranes the acyl chain connected to C1 is usually saturated with 16-18 carbon atoms while the acyl chain at C2 usually is unsaturated and has 18-20 carbon atoms.

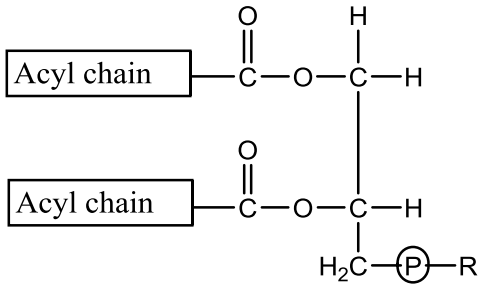

Figure 9 General structure of glycerophospholipids

Different membranes have different lipid composition due to their biological activity and the surrounding temperature. There is variation within the same membrane as the inner and outer layer in the lipid bilayer serve different purposes and also inside the leaflets as lipids tend to

aggregate into lipid rafts or lateral lipid domains (Welti and Glaser, 1994). Even though the GPLs serve as structural elements they play, in addition, important roles as second messengers and binding sites for proteins.

Cardiolipin (CL) is an anionic GPL with four acyl chains, due to linkage of two phosphate groups as shown in Figure 10, in contrast to the normal two. It is, in eukaryotes, found only in or associated with mitochondrial inner membrane and is important in energy metabolism and electron transport (Hoch, 1992; Scherer and Schmitz, 2011) and is binding site for Ca^{2+} (Nie et al., 2010). CL is protective in apoptosis as decreased CL level leads to increased cytochrome *c* release (McMillin and Dowhan, 2002). In addition it serves as site for contact of inner and outer mitochondrial membrane (Houtkooper and Vaz, 2008) and might then play an important role in mitochondrial fusion-fission cycle.

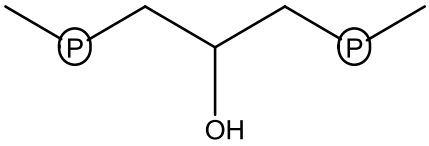

Figure 10 Molecular structure of R-group in cardiolipin

Phosphatidylcholine (PC) (structure shown in Figure 11), also called lecithin, is a zwitter ionic GPL and the most common in mammalian membranes (Niebergall and Vance, 2012). It is mainly found in the outer part of the lipid bilayer (Marconescu and Thorpe, 2008) and is more frequently localized outside the lipid rafts rather than in the rafts (Ehehalt et al., 2010). The function of several pro-inflammatory receptors tend to depend on lipid rafts and might thereby be affected by PC concentration (Ehehalt et al., 2010).

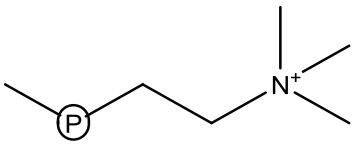

Figure 11 Molecular structure of R-group in phosphatidylcholine

Phosphatidylethanolamine (PE) (structure shown in Figure 12) is a zwitter ionic GPL and the second most common in mammalian membranes (Niebergall and Vance, 2012). It is mainly found in the inner part of the lipid bilayer, but is enriched on the surface blebs of apoptotic cells (Marconescu and Thorpe, 2008).

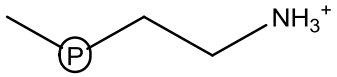

Figure 12 Molecular structure of R-group in phosphatidylethanolamine

Phosphatidylglycerol (PG) (structure shown in Figure 13) is an anionic GPL. In addition to serving as a messenger itself, PG is a substrate in the biosynthesis of CL and is, therefore, indirectly of high importance in mitochondrial function (Nie et al., 2010).

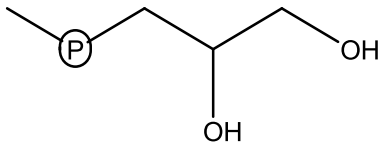

Figure 13 Molecular structure of R-group in phosphatidylglycerol

Phosphatidylinositol (PI) is an anionic GPL with a large head group (see Figure 14) and it is mainly found in the inner part of the lipid bilayer (Marconescu and Thorpe, 2008). As a result of this large head group it might contribute to a looser packaging and thereby result in a more fluidic membrane (Peng et al., 2012). PI might also have some kind of "stealth" properties as inclusion in vesicles has showed increased circulation time (Roerdink et al., 1983; Wassef and Alving, 1993). Phosphorylation might occur at position 3, 4 and/or 5 and this groups plays important roles to several proteins' activity and in generating second messengers (Farooqui et al., 2000).

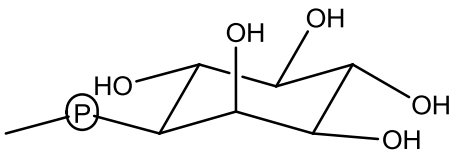

Figure 14 Molecular structure of R-group in phosphatidylinositol

2.3 Fluorescent dyes

Octadecyl rhodamine B chloride (R18) is a cationic fluorophore whose structure is shown in Figure 15. At concentration around 9 mol% relative to total lipid, R18 shows the highest effect of quenching and lower concentrations tend to be proportional with the degree of quenching (Hoekstra et al., 1984). Due to this self-quenching, R18 is a good choice of fluorescent dye for use in membrane fusion testing (Biotium, 2006) since fusion of labelled and non-labelled membranes decreases the density of R18 and thereby decreasing the effect of self-quenching, resulting in increased fluorescent intensity. Excitation wavelength for R18 used in this work was 560 nm and emission wavelength 590 nm.

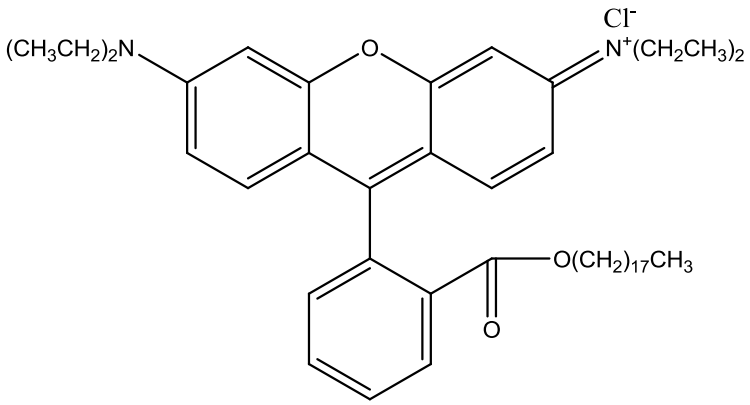

Figure 15 Molecular structure of R18 (Biotium, 2006)

Rhodamine 123 (R123) is also a cationic fluorophore whose structure is shown in Figure 16. It shows selective localization in mitochondria which is thought to be related to the opposing charges of the negative mitochondria and positive dye (Zhang and Chan, 2007). The negative charge of the mitochondria is a direct result of the membrane potential and changes will affect the fluorescent intensity of R123 (Huang et al., 2007). During exposure to cells, it tends to have a time dependent toxicity. After 10 minutes incubation no toxic effects are observed (Chen, 1989), while longer incubation cause inhibition of mitochondrial function (O'Connor et al., 1988; Hu et al., 2000). Excitation wavelength for R123 used in this work was 503 nm and emission wavelength 527 nm.

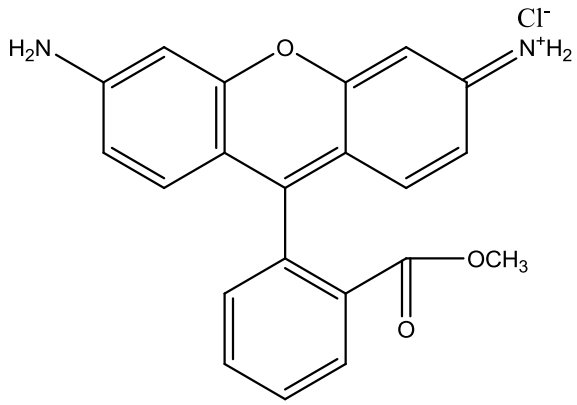

Figure 16 Molecular structure of R123 (AnaSpec, 2009)

Calcein is a hydrophilic fluorophore whose structure is shown in Figure 17. It has been shown not to interact with bilayers and not affected by pH around physiologic value, and is therefore suitable for studying liposome stability (Grit and Crommelin, 1992). It is used in encapsulation as a model for hydrophilic drugs with intermediate molecular weight (Bahia et al., 2010), however, calcein might affect the kinetics of phospholipid hydrolysis (Grit and Crommelin, 1992). Excitation wavelength for calcein used in this work was 496 nm and emission wavelength 524 nm.

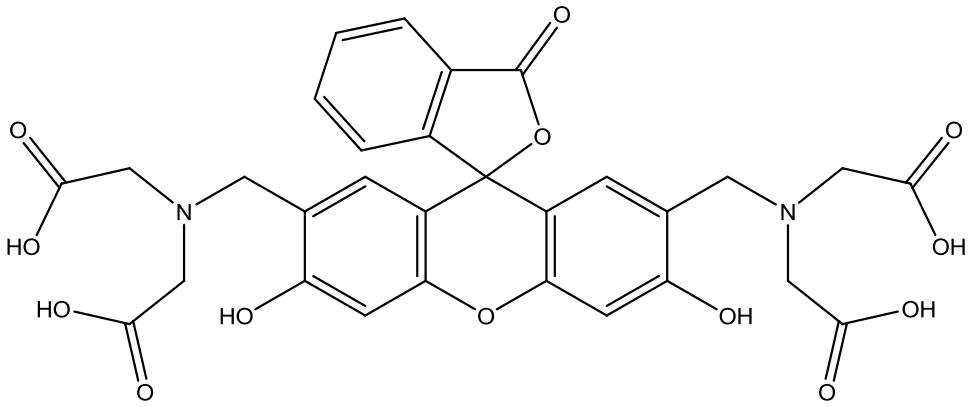

Figure 17 Molecular structure of calcein (Sigma-Aldrich®, 2006)

3 Aim of the work

Several diseases are caused by mitochondrial dysfunction. An ability to kill the responsible cells or organelles might therefor be used as a cure.

The liposomes in this work have a composition that mimics that of the outer mitochondrial membrane from Guinea-pig liver. The approach was based on their ability to be recognized as mitochondria, thus the name mito-liposomes, and be included in the fusion-fission cycle, thereby being able to act as drug delivery system targeting mitochondria.

In closer details the focus was on:

- Preparing liposomes with different lipid composition to optimize the fusion efficiency with mitochondria
- Trace the stability of the liposomes under normal storage conditions
- Isolate functional mitochondria from pig liver to test the fusion
- Preliminary experiments with encapsulation of dye to control uptake by fusion contra uptake from medium

4 Materials and Methods

4.1 Materials

4.1.1 Chemicals

Adenosine 5'-diphosphate sodium salt (ADP), Sigma-Aldrich Chemie GmbH, Steinheim, Germany

Albumin from bovine serum (BSA), Sigma-Aldrich Chemie GmbH, Steinheim, Germany

Ammonium molybdate tetrahydrate, Sigma-Aldrich Chemie GmbH, Steinheim, Germany

Calcein, Sigma-Aldrich Chemie GmbH, Steinheim, Germany

Carbonyl cyanide 3-chlorophenylhydrazone (CCCP), Sigma-Aldrich Chemie GmbH, Steinheim, Germany

Chloroform, Carl Roth GmbH, Karlsruhe, Germany

D-Mannitol, Carl Roth GmbH, Karlsruhe, Germany

D(+)-Sucrose, Carl Roth GmbH, Karlsruhe, Germany

Dimethyl sulphoxide (DMSO), Carl Roth GmbH, Karlsruhe, Germany

Ethanol (EtOH), Carl Roth GmbH, Karlsruhe, Germany

Ethylene glycol-bis(2-aminoethylether)-*N,N,N′,N′*-tetraacetic acid (EGTA), Sigma-Aldrich Chemie GmbH, Steinheim, Germany

Fiske-Subbarow-Reducer, Sigma-Aldrich Chemie GmbH, Steinheim, Germany

Hydrochloric acid 37%, Carl Roth GmbH, Karlsruhe, Germany

Hydrogen peroxide solution 31.2% (w/w), Sigma-Aldrich Chemie GmbH, Steinheim, Germany

Lipids: Cardiolipin sodium salt from bovine heart (CL), purity ≥98%, Sigma-Aldrich Chemie GmbH, Steinheim, Germany

L-α-Phosphatidylinositol ammonium salt from *Glycine max* (soybean) (SPI), purity ≥97%, Sigma-Aldrich Chemie GmbH, Steinheim, Germany

Phosphatidylcholine from egg yolk lecithin (EPC), purity ≥96%, Lipoid GmbH, Ludwigshafen, Germany

Phosphatidylethanolamine from egg yolk lecithin (EPE), purity ≥97%, Lipoid GmbH, Ludwigshafen, Germany

Phosphatidylglycerol from egg yolk lecithin (EPG), purity ≥98%, Lipoid GmbH, Ludwigshafen, Germany

Methanol (MeOH), Carl Roth GmbH, Karlsruhe, Germany

3-(N-morpholino)-propanesulfonic acid (MOPS), Carl Roth GmbH, Karlsruhe, Germany

Octadecyl rhodamine B chloride (R18), Biotium, Inc., Hayward, CA, USA

Potassium chloride, Sigma-Aldrich Chemie GmbH, Steinheim, Germany

Potassium hydrioxide, Merck KGaA, Darmstadt, Germany

Potassium phosphate dibasic trihydrate, Sigma-Aldrich Chemie GmbH, Steinheim, Germany

Potassium phosphate monobasic, Sigma-Aldrich Chemie GmbH, Steinheim, Germany

Rhodamine 123 (R123), AnaSpec, Inc., San Jose, CA, USA

Sepharose CL-4B, GE Healthcare, München, Germany

Sodium pyruvate, Biochrom AG, Berlin, Germany

Sulphuric acid, Sigma-Aldrich Chemie GmbH, Steinheim, Germany

Tetrasodium pyrophosphate, Carl Roth GmbH, Karlsruhe, Germany

Tris-(hydroxymethyl)-aminomethan (Tris), Carl Roth GmbH, Karlsruhe, Germany

Triton X-100 (Triton), Sigma-Aldrich Chemie GmbH, Steinheim, Germany

4.1.2 Tissue

Pig liver, obtained from slaughterhouse in Tullastraβe 73, D-79108 Freiburg im Breisgau, Germany

4.1.3 Working buffers and solutions

0.1 M EGTA/Tris

Ethylene glycol-bis(2-aminoethylether)-*N,N,N′,N′*-tetraacetic acid (EGTA) (1.905 g) was dissolved in Millipore water (50 ml) and pH adjusted to 7.4 with 3-(N-morpholino)-propanesulfonic acid (MOPS). Stored at 4 °C.

0.1 M Tris/MOPS

Tris-(hydroxymethyl)-aminomethan (Tris) (6.05 g) was dissolved in Millipore water (500 ml) and pH adjusted to 7.4 with Tris. Stored at 4 °C.

Isolation buffer (IB)

Sucrose (34.23 g), EGTA/Tris (5 ml 0.1 M) and Tris/MOPS (50 ml 0.1 M) were dissolved in Millipore water (total volume 500 ml) and pH adjusted to 7.4 with Tris and MOPS. Stored at 4 °C.

Respiring buffer

EGTA (0.475 g), potassium phosphate dibasic trihydrate (0.571 g), potassium chloride (4.846 g), MOPS (2.903 g) and tetrasodium pyrophosphate (0.223 mg) were dissolved in Millipore water (total volume 500 ml) and pH was adjusted to 7.15 with potassium hydroxide. BSA (0.5 g) was added prior the actual use. Stored at -80 °C.

Storage medium

Dimethyl sulphoxide (DMSO) (20 ml), sucrose (2.3961 g) and mannitol (3.8262 g) were dissolved in Millipore water (total volume 100 ml) and pH was adjusted to 7.5 with Tris and MOPS. Stored at 4 °C.

Thawing medium

Tris (0.1211 g) and sucrose (8.5575 g) were dissolved in Millipore water (total volume 100 ml) and pH was adjusted to7.5 with hydrochloric acid. BSA (0.4 g) was added prior the actual use. Stored at -80 °C.

R123 stock solution (5 mM)

Rhodamine 123 (R123) (3.808 mg) was dissolved in absolute ethanol (2 ml). Stored at -80 °C protected from light.

ADP stock solution (10 mM)

Adenosine 5'-diphosphate sodium salt (ADP) (4.27 mg) was dissolved in Millipore water (1 ml). Stored at -80 °C protected from light.

CCCP stock solution (4 mM)

Carbonyl cyanide 3-chlorophenylhydrazone (CCCP) (8.18 mg) was dissolved in 10 ml absolute ethanol. Stored at -80 °C.

IB-calcein (10 mM)

Calcein (124.5 mg) was dissolved in IB (20 ml) and pH adjusted to 7.4 with Tris. Stored at 4 °C protected from light.

4.1.4 Equipment

Concentrator: 5301, Eppendorf AG, Hamburg, Germany

Hand extruder: LiposoFast-Basic, Avestin, Inc., Ottawa, Canada

Zetasizer: Zetasizer Nano S, Malvern Instruments Ltd, Worcestershire, UK

UV/visible spectrophotometer: Ultrospec 1000, Parmacia Biotech Biochron, Cambridge, UK

Copper grid: Quantifoil® S7/2 Cu 400 mesh, holey carbon films, Quantifoil Micro Tools GmbH, Jena, Germany

Cryo-sample container: Model 626-DH, Getan, Inc., Warrendale, Pennsylvania, USA

Transmission-electron microscope: Leo 912 Ω-mega, LEO Electronenmikroskopie GmbH, Oberkochen, Germany

Transmission-electron microscope: iTEM 5.0 (Build 1054), Olympus Soft Imaging Solutions GmbH, Münster, Germany

Cryo-camera: Cryo-Box 340719, Carl Zeiss MicroImaging GmbH, Jena, Germany

Camera TEM: Proscan HSC 2, Oxford Instruments, Abingdon, UK

Photon correlation spectroscopy: Zeta Potential Analysis, Brookhaven, New York, USA

Fluorometer: Fluorescence Spectrometer LS 55, Perkin Elmer, Waltham, Massachusetts, USA

Homogenizer: 50 ml glass potter with Teflon pestle, Fisher Scientific, Pittsburgh, Pennsylvania, USA

Centrifuge: 5804 R, Eppendorf AG, Hamburg, Germany

Centrifuge: Avanti® J-E, Beckman Coulter, Brea, California, USA

Protein concentration kit: *DC* Protein Assay, Bio-Rad Laboratories, Inc., Hercules, California, USA

SpectraCount™: BS10001, Packard, now: Perkin Elmer, Waltham, Massachusetts, USA

Thermomixer: Thermomixer comfort, Eppendorf AG, Hamburg, Germany

4.2 Methods

4.2.1 Liposome preparation

The liposomes were made by the film method (Torchilin and Weissig, 2003). The lipids and the R18 in the amounts as listed in Table 1 were prepared as aliquots and thereby dissolved in a mixture of chloroform and methanol (volume ratio 9:1) in a round bottom flask and placed on a rotary evaporator to remove the solvent. The water bath was set to 40 °C and the pressure was slowly decreased to 260 mBar until a visible lipid film was formed on the bottom of the flask. After 10 minutes at 260 mBar the pressure was further decreased to 0 mBar and let to stand for 1 hour.

R18 mito-lipo 1 have the same lipid composition as OMM (Daum, 1985).

Table 1 Lipid composition of the different R18 mito-lipos

Preparation name	**Composition** [molar ratio]					
	R18	**PC**	**PE**	**PI**	**PG**	**CL**
R18 mito-lipo 1	7.50	51.83	24.44	11.93	2.84	1.47
R18 mito-lipo 2^-	3.30	-	24.44	11.93	2.84	1.47
R18 mito-lipo 3^-	5.52	51.83	-	11.93	2.84	1.47
R18 mito-lipo 4^-	6.53	51.83	24.44	-	2.84	1.47
R18 mito-lipo 5^-	7.27	51.83	24.44	11.93	-	1.47
R18 mito-lipo 6^-	7.38	51.83	24.44	11.93	2.84	-
R18 mito-lipo 2^+	11.70	103.66	24.44	11.93	2.84	1.47
R18 mito-lipo 3^+	9.48	51.83	48.88	11.93	2.84	1.47
R18 mito-lipo 4^+	8.47	51.83	24.44	23.86	2.84	1.47
R18 mito-lipo 5^+	7.73	51.83	24.44	11.93	5.68	1.47
R18 mito-lipo 6^+	7.62	51.83	24.44	11.93	2.84	2.94

The rehydration of the films was done by adding 4 glass balls ($\Phi \approx 2$ mm) together with a specific volume of IB according to a lipid concentration of approximately 5 mM. The flask was placed at rotary evaporator for 20 minutes. If there were visible aggregates the flask was placed in sonication bath for a few seconds. After removal of the glass beads, the suspension was extruded through a 200 nm polycarbonate membrane 21 times, followed by extrusion through a 100 nm polycarbonate membrane 21 times and finally through a 50 nm

polycarbonate membrane 31 times. The liposomes were stored at 4 °C protected from light till further experiments.

Samples were evaluated for total phosphorous content by Bartlett assay (Bartlett, 1959) and cryo-transmission-electron microscopy studies in addition to determination of particle size, fluorescent intensity and zeta potential.

To determine the encapsulation efficiency for calcein, the lipid films was made in the same way as described above without inclusion of R18. The rehydration buffer used was IB-calcein. A step with 3 times freeze-thaw cycles was added to increase the encapsulation efficiency, in which the liposomal suspension was frozen in liquid nitrogen, thawed in 25 °C water bath for 5 minutes and thoroughly mixed. The suspension was then extruded only through a 200 nm polycarbonate membrane 21 times.

4.2.2 Encapsulation efficiency

After extrusion, the calcein containing liposomes was separated from un-entrapped calcein on a Spharose CL-4B/IB column. Liposome fractions were evaluated by Bartlett assay (Bartlett, 1959).

To determine the encapsulation efficiency, the fluorescence intensity of 0% and 100% samples were used as standards. For the 0% value 10% (w/w) Triton (100 µl) was diluted with IB (total weight of 10 g). For the 100% value Triton (100 µl 10% (w/w)) and non-separated sample (100 µl) were diluted with IB (total weight 10 g). The further dilutions of the samples were prepared by diluting 100% sample until the fluorescent intensity was approximately 800-900.

For the encapsulation determination, the liposome fraction, after separating sample (100 µl), was diluted with IB (total weight 10 g) including Triton (100 µl 10% (w/w)). The same dilutions as for 0% and 100% were prepared and the fluorescent intensities used to calculate the efficiency of the encapsulation by the following formula:

$$\text{Encapsulation efficiency} = \frac{F_{sample} - F_{0\%}}{F_{100\%} - F_{0\%}} \qquad \text{Eq. 1}$$

Where F_{sample} represents the fluorescence intensity of the liposome fraction, $F_{0\%}$ represents the fluorescence intensity of the 0% standard and $F_{100\%}$ represents the fluorescence intensity of the 100% standard.

4.2.3 Characterization of liposomes

4.2.3.1 Determination of zeta potential

Liposome suspension (0.5 ml 5 mM) was diluted in IB (0.5 ml) and transferred to a conductive cuvette. The measurements were performed at room temperature. The average of 3 runs was calculated, each consisting 15 zeta runs.

The refractive index of the IB was 1.340 and the viscosity was 1.0939 cP (Zhou, 2012). The dielectric constant was kept at 78.5.

4.2.3.2 Total phosphorous content – Bartlett assay (Bartlett, 1959; Zhou, 2012)

A potassium phosphate monobasic calibration curve was made with concentration ranging from 50 to 350 nmol. Three tubes without any phosphor were used as blanks. Sulphuric acid (0.5 ml 10 N) was added to each tube before incubation at 160 °C. After 3 h hydrogen peroxide solution (200 µl 31.2% (w/w)) was added and the incubation continued for another 1.5 h. Ammonium molybdate solution (4.5 ml 0.22% (w/V)) and Fiske-Subbarow-Reduces solution (200 µl 14.8% (w/V)) were added to each tube. The solutions was then mixed using vortex mixer before further incubation at 95 °C for 10 minutes. After cooled down to room temperature the samples were photometric measured at λ = 830 nm.

4.2.3.3 Cryo-transmission-electron microscopy (Zhou, 2012)

Liposome suspension (3 µl 5 mM) was applied to a copper grid and excessive fluid was removed with filter paper prior to immediately freezing using liquid ethane. The grid was then fixed in a cryo-sample container and inserted in the transmission-electron microscope which operated with an acceleration voltage of 120 kV. The pictures were taken with a corresponding camera with magnifications ranging from 6300 times to 12500 times.

4.2.3.4 Stability testing

Control experiments were performed to evaluate the stability of the liposome suspensions upon storage in 4 °C. The control experiments were done after preparation and after 1 week, 2 weeks, 3 weeks, 4 weeks, 2 months, 3 months and 4 months.

Photon correlation spectroscopy (PCS) was used to measure the effective, or hydrodynamic, diameter in order to detect possible liposome fusion. The measurements were performed at room temperature. Liposome suspension (30 µl 5 mM) was added to sterile filtrated IB (1000 µl). The count rate was kept between 50 and 60 kcps and the polydispersity was kept bellow 0.1. Each run lasted 10 minutes and consisted of 5 sub runs.

A fluorescence spectrometer was used to measure the fluorescence intensity in order to detect possible leakage of R18 from the liposomes into the IB. Liposome suspension (5 µl 5 mM) was added to sterile filtrated IB (2500 µl). The measurements were performed at room temperature and three parallels were noted.

4.2.4 **Isolation of mitochondria** (Frezza et al., 2007; Zhou, 2012)

Fresh pig liver was brought in ice bath from the slaughterhouse and was kept in ice during all preparatory steps. The IB and all centrifugation tubes containing tissue homogenate between the centrifugations were also kept in ice bath. During all centrifugations the temperature was kept at 4 °C.

The liver was washed in IB and minced while continuously being hydrated with IB. The minced liver was immersed in IB and centrifuged to remove blood. After starting the centrifuge, rotation was manually stopped when the speed reached 500 g. The supernatant containing the blood was discarded and the process was repeated 2-3 more times until the supernatant appeared almost colourless. Connective tissue was removed using forceps before diluting with IB in a ratio 4:1 (IB : minced tissue, w/w) for further homogenization in a 50 ml precooled glass potter with Teflon pestle. The glass potter was kept on ice and raised/lowered 3-4 times with a pestle speed of 1600 rpm, as demonstrated in Figure 18. The homogenate was centrifuged at 600 g for 10 minutes to precipitate cellular fragments and organelles larger than the mitochondria. The supernatant was collected and centrifuged at 7000 g for 10 minutes to precipitate the mitochondria. The supernatant was discarded, and the pellet re-suspended in IB. The process was repeated 2 more times. After the last centrifugation, the pellet was kept in a concentrated from to preserve the quality of the mitochondria. The concentration was measured by protein assay and the viability tested by dye-time course.

Figure 18 Illustration photo of homogenization of tissue
(Photo: Else Mari Ødegaard-Jensen)

4.2.5 **Freezing and thawing** (Zhou, 2012)

Both tissue and isolated mitochondria were kept frozen in liquid nitrogen and stored at -80 °C if not used immediately. The mitochondria did not require any pre-handling, but the tissue was first washed in storage medium.

In order to use the frozen tissue, the thawing medium was first pre-warmed to 45 °C (tissue : thawing medium in ration 1:4) and added directly to the frozen tissue. The tissue was agitated or stirred in the thawing medium in order to fasten the thawing process. After complete thawing of the tissue, it was kept on ice during the isolation as described earlier.

The frozen isolated mitochondria were thawed by holding the tube manually or through use of 37 °C water bath until completely thawed. The tube was then placed on ice.

4.2.6 Viability testing

4.2.6.1 **Protein concentration assay** (Bio-Rad)

The measurements were done at room temperature and on a microplate.

For standard curve 3-5 dilutions of BSA were prepared in IB with concentration ranging between 0.2-1.5 mg/ml. The mitochondria sample was diluted to desired concentrations. BSA standard dilutions (5 µl) and sample dilutions (5 µl) were transferred to microplate. *Reagent A* (25 µl) and *Reagent B* (200 µl) were added into each well. After gentle agitation, the plate was left for 15 minutes protected from light at room temperature for reaction to take place. The absorbance was detected at 750 nm using SpectraCount. The protein concentration detected in standard samples equals the concentration of mitochondria.

4.2.6.2 **Dye-time course** (Huang et al., 2007; Zhou, 2012)

The measurements were done at 37 °C (physiological temperature).

R123 (2.5 µl 35 µM) and sodium pyruvate (250 µl 100 mM) were added to a cuvette containing magnetic stirrer and respiring buffer (2247.5 µl). After a few minutes, allowing the fluorescence intensity to stabilize, isolated mitochondria (25 µl 100 mg/ml; 1 mg/total ml) was added and a drop in fluorescent intensity observed due to self-quenching resulting from attractions between positive dye (see Figure 16) and negative mitochondria. After the fluorescence intensity was stabilized, ADP (25 µl 10 mM) was added and an increase in fluorescent intensity observed due to changed membrane potential resulting from condensation of ADP and inorganic phosphate into ATP. If the mitochondria were able to synthesize ATP, a drop in fluorescent intensity was observed when all the ADP was used. After the fluorescence intensity was stabilized, CCCP (2.5 µl 4 mM) was added as a control and a drastic increase in fluorescent intensity was due to uncoupling of the respiratory chain.

4.2.7 **Fusion experiment** (Zhou, 2012)

To determine the encapsulation efficiency, the fluorescence intensity of 0% and 100% samples were used as standards. Both the 0% and the 100% was incubated in a thermomixer controlled at 37 °C and with a speed of agitation of 700 rpm for 5 minutes before the fluorescent intensity was measured. For the 0% value R18 mito-lipo suspension (10 µl 1mM) was added to IB (1990 µl). For the 100% value R18 mito-lipo suspension (10 µl 1mM) and Triton (100 µl 10% (w/w)) was added to IB (1890 µl).

To determine the fusion efficiency R18 mito-lipo suspension (10 µl 1mM) and isolated mitochondria (20 µl 100 mg/ml; 1 mg/total ml) were added to IB (1970 µl) and incubated at 37 °C in a thermomixer with a speed of agitation of 700 rpm for 45 minutes before measuring the fluorescent intensity. The fluorescent intensities observed were used to calculate the efficiency of the fusion by the following formula:

$$\text{Fusion efficiency} = \frac{F_{fusion} - F_{0\%}}{F_{100\%} - F_{0\%}} \qquad \text{Eq. 2}$$

Where F_{fusion} represents the fluorescence intensity of the fused mito-lipo/mitochondria suspension, $F_{0\%}$ represents the fluorescence intensity of the 0% standard and $F_{100\%}$ represents the fluorescence intensity of the 100% standard.

5 Results and discussion

5.1 Liposome characterization

The control of particles size in drug delivery is important in order to avoid removal by MPS (Brandl, 2001). In addition, sedimentation of particles related to gravity will decrease with decreasing size of particles. The liposome suspensions were prepared having a mean size around 100 nm and the polydispersity was used as a measure of vesicle size distribution. As shown in Table 2, the sizes of liposomes were close to 100 nm and the polydispersities were below 0.1, which indicates a narrow size distribution. The exception was R18 mito-lipo 4^-, however, similar results were reported previously (Zhou, 2012).

Table 2 Physical properties of R18 mito-lipos

	Effective diameter (n = 5)		Polydispersity (n = 5)		Zeta potential (n = 3)	
	Size [nm]	SD [nm]	p.i.	SD	ζ [mV]	SD [mV]
R18 mito-lipo 1	101.0	1.5	0.056	0.004	-35.8	15.4
R18 mito-lipo 2^-	109.4	0.4	0.064	0.010	-43.6	14.6
R18 mito-lipo 3^-	101.4	0.4	0.045	0.012	-50.1	14.5
R18 mito-lipo 4^-	125.0	0.9	0.173	0.008	-5.5	4.0
R18 mito-lipo 5^-	102.2	0.6	0.066	0.017	-46.0	11.7
R18 mito-lipo 6^-	106.3	0.7	0.055	0.006	-42.1	11.0
R18 mito-lipo 2^+	99.5	0.4	0.069	0.012	-25.0	14.5
R18 mito-lipo 3^+	99.5	0.6	0.076	0.014	-31.9	14.3
R18 mito-lipo 4^+	97.6	1.7	0.045	0.012	-42.7	17.5
R18 mito-lipo 5^+	93.8	0.6	0.037	0.012	-39.6	15.9
R18 mito-lipo 6^+	100.8	0.8	0.053	0.008	-39.7	15.7

Zeta potential can be used as a measure for the stability of liposome suspension; an increase in the absolute value of zeta potential decreases the probability of particle agglomeration (Zanatta et al., 2010). Zeta potential has also been linked to opsonization as it is known that a zeta potential value close to neutral makes the particle less prone to opsonization and thereby results in prolonged circulation time of particle (Kaasalainen et al., 2012).

Zeta potential has been shown to affect the membrane interactions between cells and non-specific nanoparticles where positive charged shows enhanced uptake due to the opposite charge of the cell membrane (Kaasalainen et al., 2012). According to this, R18 mito-lipo 4^-

would be expected to have the highest fusion efficiency since it had the least negative charge (Table 2).

The actual lipid concentration was measured in order to assure an accurate and comparable volume of liposome suspension in the fusion experiments. For the R18 mito-lipos, the results are listed in Table 3 and the actual concentration were found to be close to the theoretical values.

Table 3 Phospholipid content in R18 mito-lipos

	Theoretical concentration [mM]	Actual concentration [mM]
R18 mito-lipo 1	5.0	4.9
R18 mito-lipo 2^-		4.5
R18 mito-lipo 3^-		4.7
R18 mito-lipo 4^-		4.7
R18 mito-lipo 5^-		4.8
R18 mito-lipo 6^-		4.7
R18 mito-lipo 2^+		5.1
R18 mito-lipo 3^+		5.0
R18 mito-lipo 4^+		5.1
R18 mito-lipo 5^+		4.6
R18 mito-lipo 6^+		4.9

Bartlett assay used in determination of phospholipid is determining the total amount of phosphor in the sample and it is limited in determination of the relative amount of the different lipids present in the liposomal formulation. This is a result of the process of turning lipid phosphate groups to free phosphate (Bartlett, 1959; Mrsny et al., 1986). During the preparation of liposomes, problems regarding aggregation with some of the liposome suspensions led to need for additional sonication in order to obtain homogenous suspensions. Due to the colour of the aggregates, it appeared that it was mostly due to un-dissolved R18. When liposomes were prepared without any fluorescent dye (data not shown) there were no visible aggregates. However, this does not exclude the possibility that the lipids are unevenly distributed throughout the liposome membranes and between the liposomes in the suspensions. An uneven distribution might cause problems or variability during fusion experiments. Still, there is no straightforward way to confirm a homogenous lipid distribution and it must therefore be assumed that lipid distribution was even.

Micrographs of the liposome suspensions were taken in order to evaluate the shape of the liposomes. We wanted to follow possible morphological alterations as a result of different lipid compositions of liposomes and the alterations in membrane structure which was expected to affect membrane fusion (Roy et al., 2010). Comparison of liposomes with different lipid concentration were made, with particular emphasis on the absence of specific lipids (Figure 19) relative to double amount of the same lipid (Figure 20) related to effect of fusion.

All preparations showed irregular liposomes with large cavities, but R18 mito-lipo 1 was thought to contain the most spherical particles. There were also particles of very small sizes that might result from the use of 50 nm membrane during extrusion.

For liposomes containing doubled amounts of PC (Figure 20b), PG (Figure 20e) and CL (Figure 20f) high numbers of disc-like liposomes were observed. For PG liposomes, in addition, a more regular shape was seen than when PG was absent (Figure 19e), possibly due to a stabilizing effect of hydrogen bonds, and for CL liposomes, a more uniform size than when CL was absent (Figure 19f). On the other hand, when PC was absent from the preparation it tend to contain more spherical particles (Figure 19b).

Double amount of PI present in liposomes (Figure 20d) appears to have smaller cavities and more regular shape than when PI was absent (Figure 19d). This might be related to the large head group of PI as it can cause steric hindrance and thereby reduce the presence of cavities, or generation of hydrogen bonding to neighbouring lipids and/or buffer (Peng et al., 2012). When the amount of PE was double (Figure 20c) it showed fewer cavities than when PE was absent (Figure 19c) but the shape of the particles was more irregular.

Sterols and proteins are present in biological membranes where they appear to have a membrane stabilizing role (Churchward and Coorssen, 2009; Roy et al., 2010). The prepared liposomes did not contain such stabilizers which might be one explanation to the folds and cavities in the particles, in addition to possible destabilizing properties of the lipids.

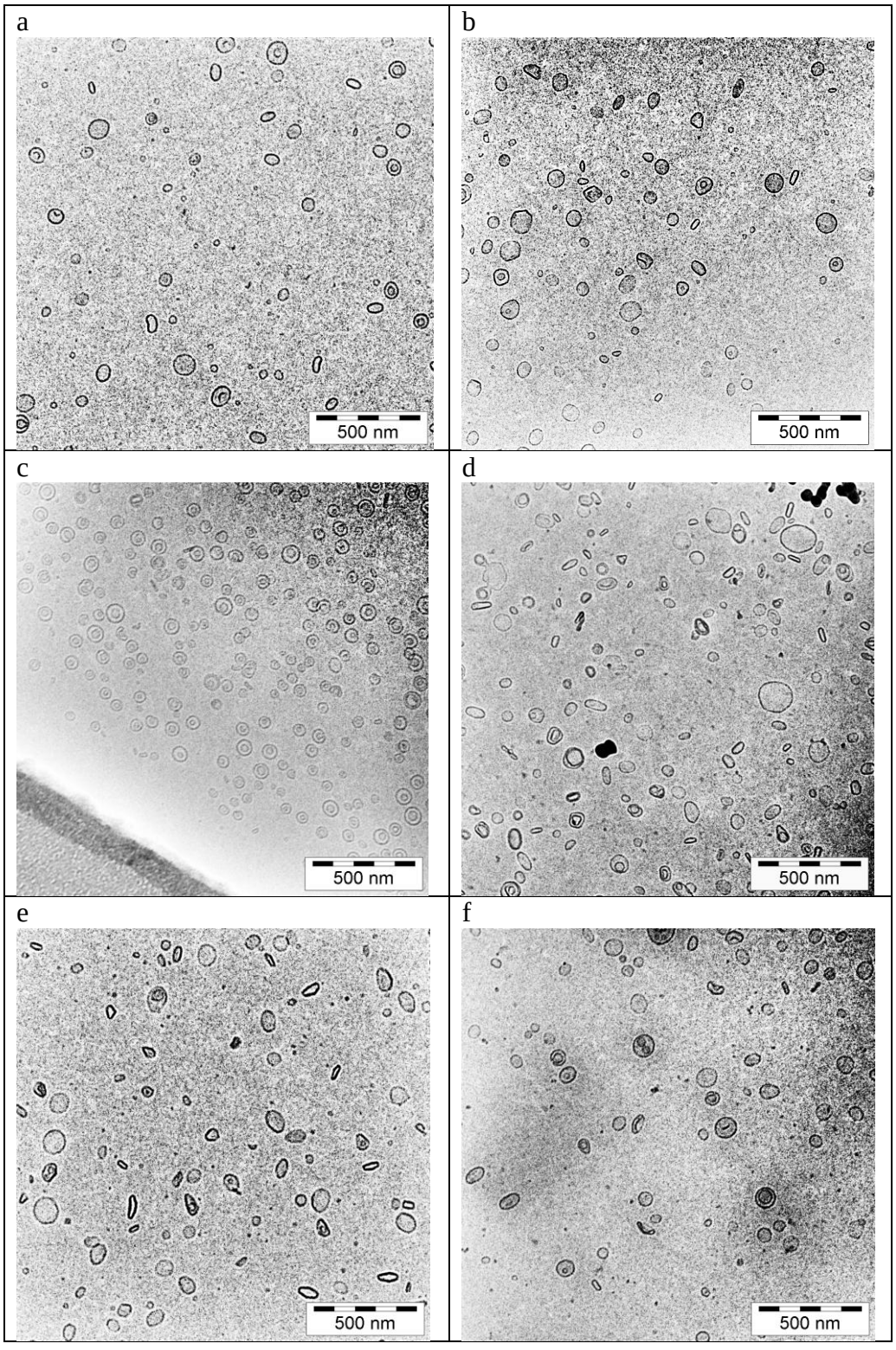

Figure 19 Cryo-Transmission-Electron micrographs of liposomes lacking specific lipids:
a) R18 mito-lipo 1; b) R18 mito-lipo 2^-; c) R18 mito-lipo 3^-;
d) R18 mito-lipo 4^-; e) R18 mito-lipo 5^-; f) R18 mito-lipo 6^-

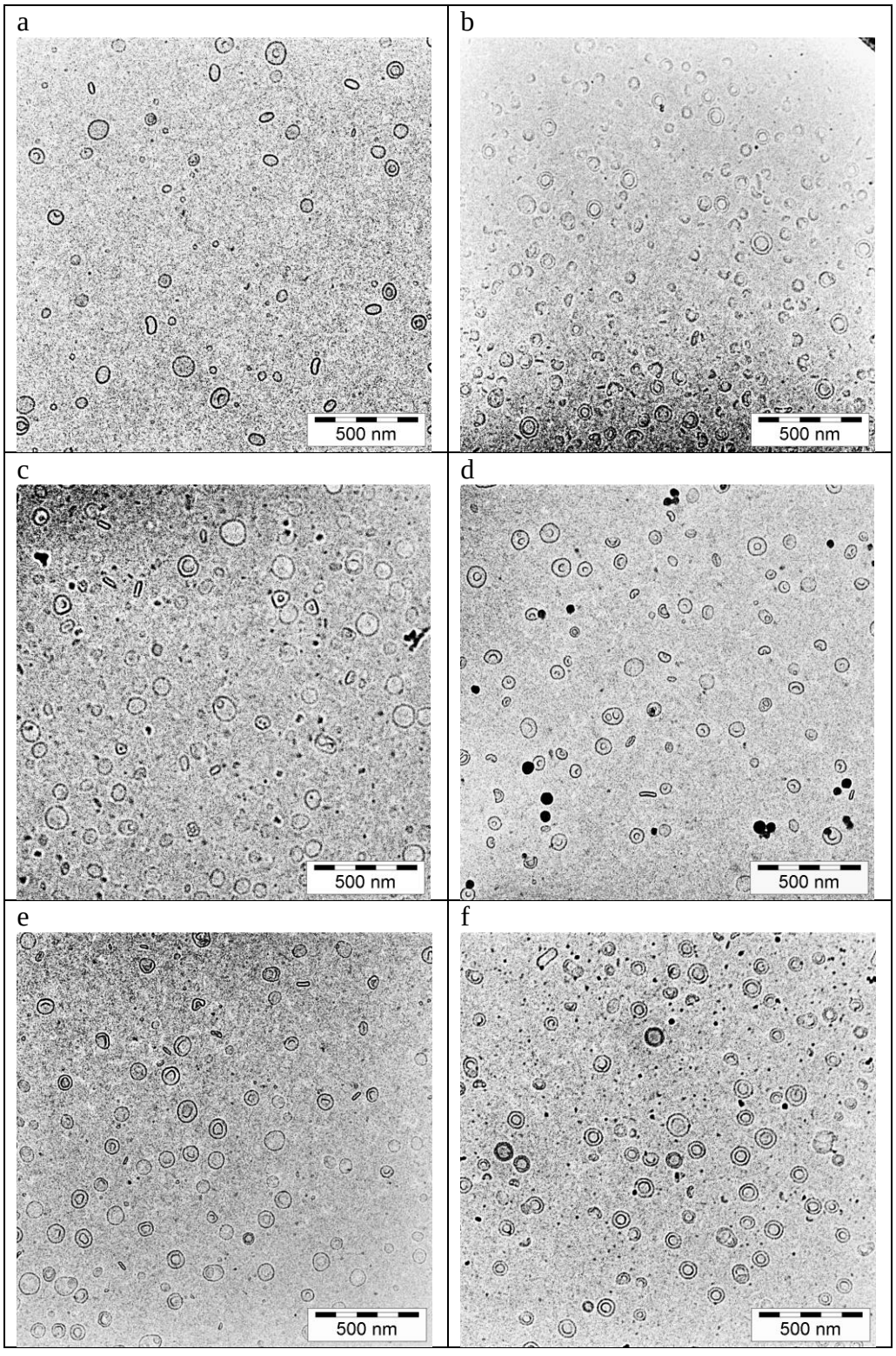

Figure 20 Cryo-Transmission-Electron micrographs of liposomes with doubled amount of specific lipids:
a) R18 mito-lipo 1; b) R18 mito-lipo 2^+; c) R18 mito-lipo 3^+;
d) R18 mito-lipo 4^+; e) R18 mito-lipo 5^+; f) R18 mito-lipo 6^+.

5.2 Stability testing of liposomes

Liposome suspensions are prone to two types of degradation, namely hydrolysis and oxidation (Brandl, 2001). As stability of the lipid bilayer is reduced when the lipids are degraded (Grit and Crommelin, 1992), change in particle size and fluorescence intensity will reflect loss of stability.

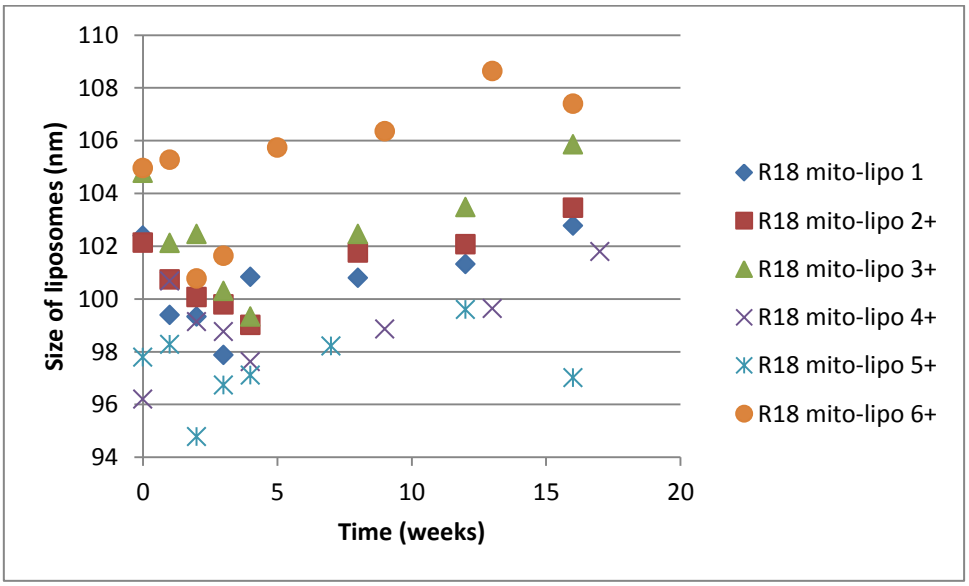

Figure 21 Changes in mean liposome size over four months period

As Figure 21 indicates, there were some fluctuations in particle size, but from a general view the liposomes keep stable. During the storage period no sedimentation was visible, but that does not exclude the possibility of uneven distribution throughout the suspension which would result in fluctuations as observed. There occurred problems during some of the sampling which led to repetition of some measurements. If it was due to the sampling itself or the problems with the apparatus was not clear.

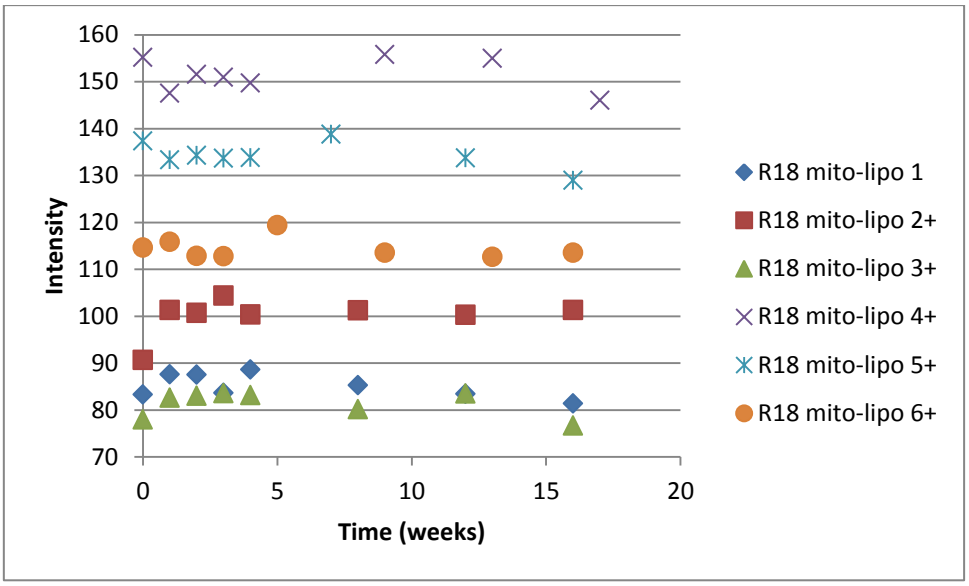

Figure 22 Changes in R18 fluorescence intensity over four months period

Figure 22 shows that the self-quenching effect of R18 was stable throughout the storage period. The fluorescent intensity is highly susceptible to changes in both relative dye concentration and sample temperature (Trikash et al., 2010). Combined, this suggests that the liposomes keep stable in suspension and due to the sensitivity, fluorescent intensity might be a more reliable method for evaluating the stability than the size determination.

The liposomes appeared to retain the incorporated dye under normal storage conditions (4 °C and protected from light) for at least four months. However, how much of active ingredient, such as drug or protein, will be retained when encapsulated or incorporated cannot be directly extrapolated.

Stability of R18 mito-lipos without specific lipids was not evaluated since previous evaluation has shown them to be stable (Zhou, 2012). Due to the low zeta potential of R18 mito-lipo 4^- it would be expected that the vesicles are unstable, but that was not the case.

5.3 Viability testing of mitochondria

In order to obtain reliable results when studying mitochondrial functions it is important to use well-respiring organelles (Frezza et al., 2007). There are several methods for purification of mitochondria, but purity and viability have to be estimated (Hornig-Do et al., 2009). To evaluate the viability of the isolated mitochondria, the concentration had to be known and protein concentration in the samples (listed in Table 4) was used as a measure for the mitochondrial concentration.

Table 4 Protein concentration of isolated mitochondria

	Protein concentration (n = 3)	
	Protein [mg/ml]	SD [mg/ml]
Isolation from fresh tissue	94.11	3.45
Isolation from frozen tissue (thawed and minced with knife)	52.74	2.62
Isolation from frozen tissue (not thawed and minced with grinder)	48.82	2.00

Isolation of mitochondria from fresh tissue was performed together with a well-trained personal and the processes were thereby performed at a higher speed. That might be the main reason for the high yield. When the isolations were performed from frozen tissue, the process was slower which might be the cause both the lower yield and decreased respiration.

Dye-time course is based on the accumulation of R123 in MM, and thereby self-quenching effect, according to mitochondrial membrane potential (Huang et al., 2007). Changes in membrane potential leads to altered uptake of R123, resulting in a proportional change in fluorescent intensity.

The mitochondria isolated from fresh tissue (Figure 23) showed decreased viability after storage (Figure 24). They also appeared to be non-respiring when isolated from frozen tissue (Figure 25 and Figure 26). This may as well be a result of slow experimental handling rather than the actual storage since previous (unpublished) experiments have also shown reduced viability with increased time used for isolation. It is evident that it is highly recommendable to use the mitochondria as soon as possible after isolation, as time affects their viability.

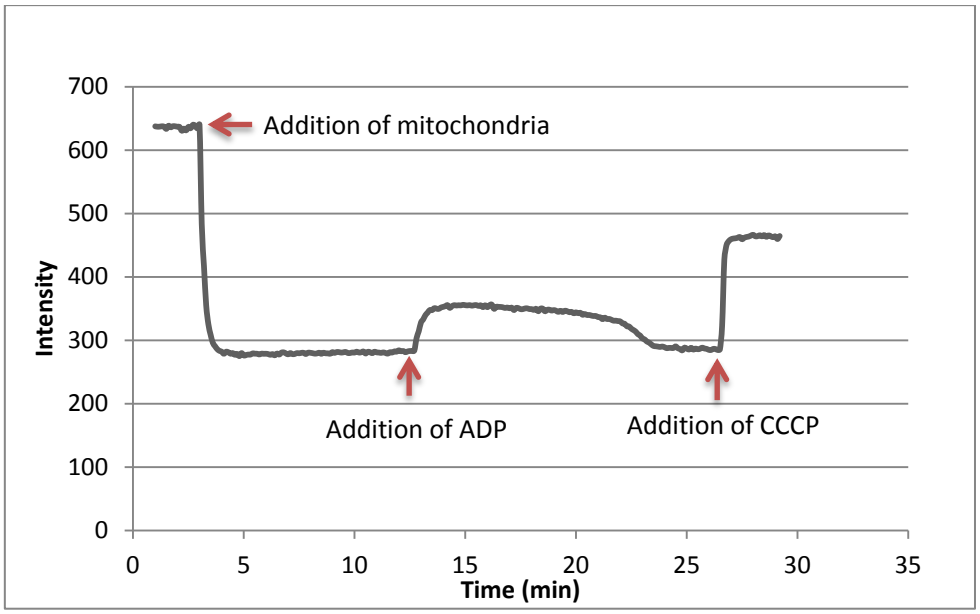

Figure 23 Dye-time course of mitochondria directly after isolation

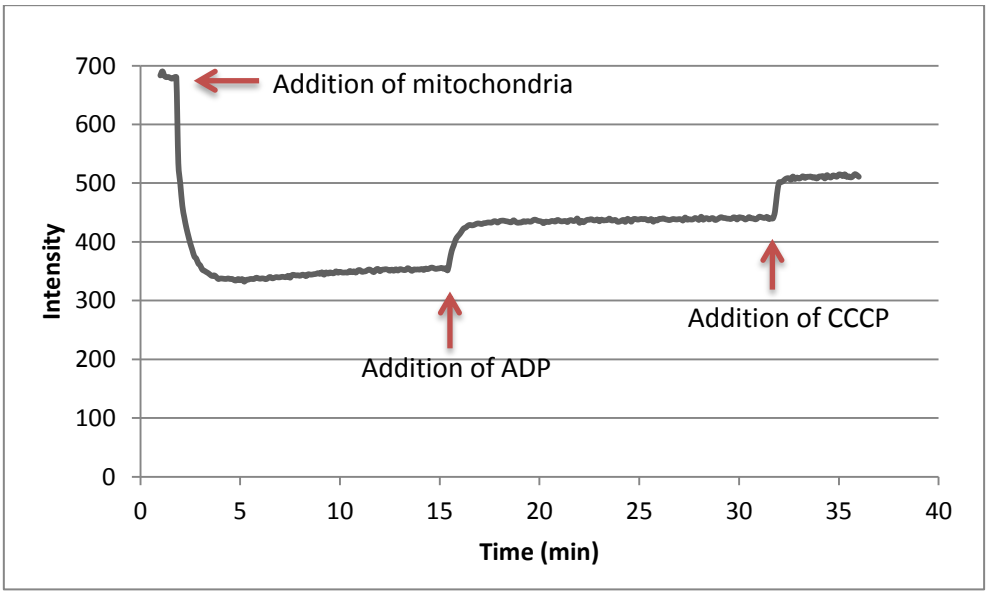

Figure 24 Dye-time course of mitochondria before fusion experiment: frozen in liquid nitrogen and stored in -80°C

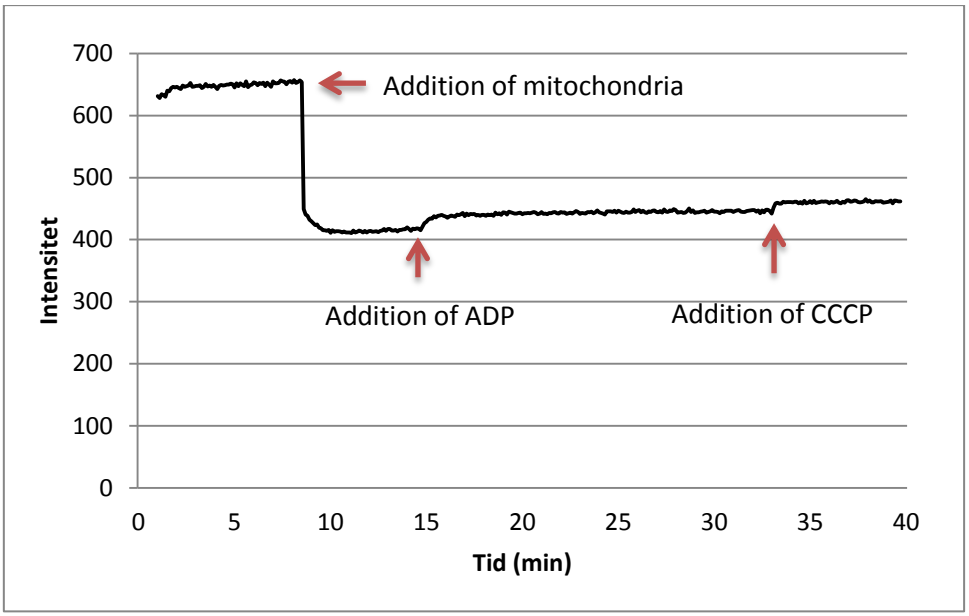

Figure 25 Dye-time course of mitochondria isolated from frozen tissue: thawed and minced with knife

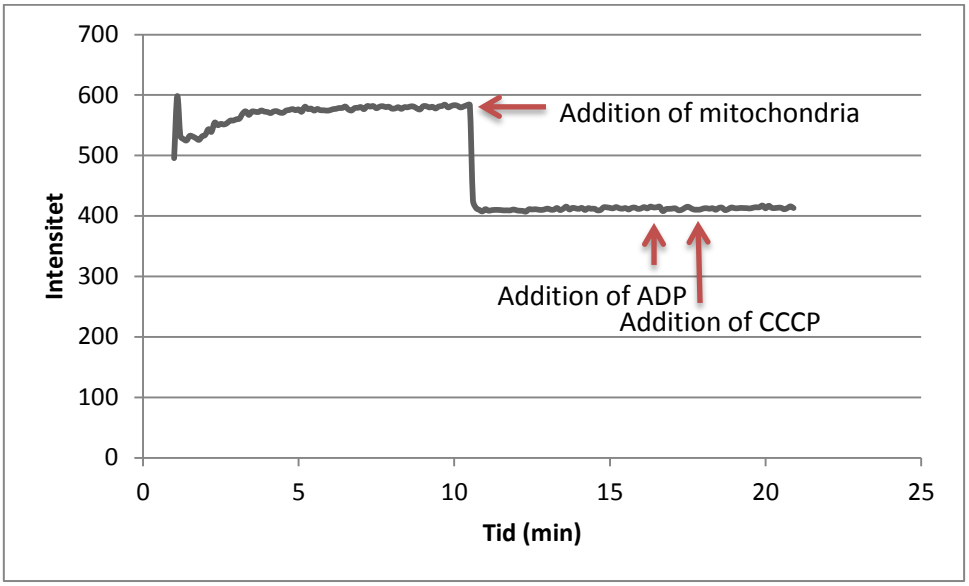

Figure 26 Dye-time course of mitochondria isolated from frozen tissue: not thawed and minced with grinder

5.4 Fusion experiment

The results from the fusion experiment are summarized in Figure 27, where the fusion efficiencies are illustrated relative to the fusion result for R18 mito-lipo 1. R18 mito-lipo 1 was chosen as a baseline since it had the same composition as the OMM and is, according to the hypothesis, recognized as a mitochondrion and included in the fusion-fission cycle.

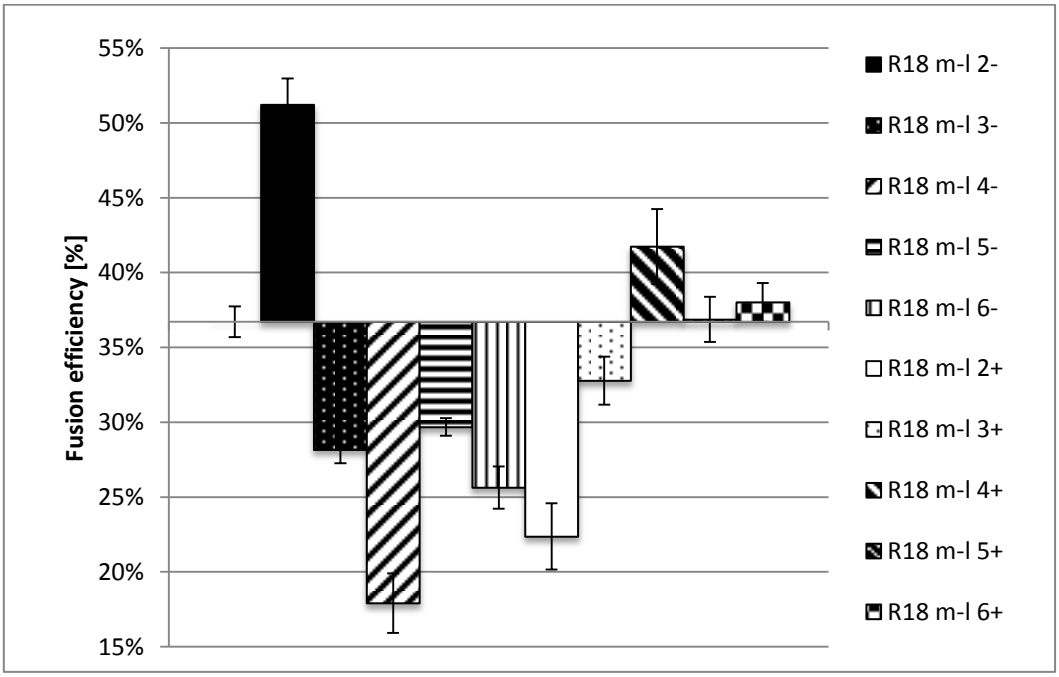

Figure 27 Fusion efficiency of R18 mito-lipos with altered lipid composition relative to R18 mito-lipo 1. X-axis show the fusion efficiency of R18 mito-lipo 1, with the standard deviation bars at the very left being the standard deviation for R18 mito-lipo 1

When PC was absent the fusion efficiency was increased, and when it was doubled the fusion efficiency decreased. As the most common lipid in mammalian membranes, PC would be expected to have positive, or at least neutral, effect on the fusion process. However, the results showed a clear inhibitory effect. At this point of the project, it is difficult to provide deeper insight on why PC is inhibiting rather the improving fusion process.

On the other hand, when PI was removed the fusion efficiency was decreased, and when it was doubled the fusion efficiency increased. This indicates that PI plays an enhancing role in the fusion process. The expected increased ability to fuse for R18 mito-lipo 4^- due to its zeta potential did for sure not occur as it had the lowest fusion efficiency of all, and the data are

very clear. One possible reason why the theory proposed by Kaasalainen and co-workers does not correspond to the results presented here might be the complexity of the liposomes (Kaasalainen et al., 2012). They were not non-specific in nature but were rather made to mimic the composition of the mitochondrial membrane, which can be considered as targeting composition. Another possible explanation might be related to the large head group of PI (Figure 14). Peng and co-workers showed that inclusion of PI resulted in deeper water penetration in the membrane, however, they stated that the lipid had inhibitory effects in fusion (Peng et al., 2012). In our case, the opposite was seen.

The other lipids seemed to have little or no specific effect on the fusion as they were in more or less the same region of the scale (Figure 27). However, a slight increase in fusion efficiency was observed in liposome preparations containing CL relative to when it was removed. Since CL is associated with proteins in ETC and OMM receptors and channels (Schug and Gottlieb, 2009), it acts as site for contact of inner and outer mitochondrial membrane (Houtkooper and Vaz, 2008), and also plays a role in apoptosis where decreased CL level lead to increased cyt c release (McMillin and Dowhan, 2002). It might therefore be an important vehicle component for drug delivery to mitochondria.

When comparing Figure 19 and Figure 20 in respect to R18 mito-lipo 2^- and 2^+ and R18 mito-lipo 4^+ and 4^-, which are the liposomes with the highest and the lowest fusion, respectively, it can be concluded that liposomes tend to have a more spherical shape when they are able to fuse better. This is a theory supported by previous research as well (Roy et al., 2010). For the other samples it appeared that a more uniform size and shape, independent of the actual shape, improved fusion.

5.5 Encapsulation efficiency

Based on the results in Figure 27 the R18 mito-lipo 1, R18 mito-lipo 2^- and R18 mito-lipo 4^+ were selected to be used for further experiments. Calcein was encapsulated in order to compare delivery via fusion and direct uptake from buffer to evaluate the efficiency of fusion delivery.

The liposomes with encapsulated calcein were bigger than the R18 mito-lipos. This was to assure that calcein would pass the extrusion membrane and that it would stay inside the liposomes. As shown in Table 5, the size distribution of the liposomes was narrow.

Table 5 Physical properties of Mito-lipos

	Effective diameter (n = 5)		Polydispersity (n = 5)	
	Size [nm]	SD [nm]	p.i.	SD
Mito-lipo 1	216.8	3.1	0.069	0.012
Mito-lipo 2^-	256.0	4.7	0.042	0.006
Mito-lipo 4^+	266.9	1.3	0.073	0.016

The actual lipid concentrations for the Mito-lipos are listed in Table 6 and it seems that there was no lipids present in Mito-lipo 2^-. However, results in Table 5 indicate the presence of particles in the sample, moreover, particles with the expected size. The explanation for this discrepancy could be in a fact that the separation of un-encapsulated dye from liposome fraction was hard to perform as liposome fraction on the column appeared almost colourless. In Mito-lipos 2^- there was no coloured band visible on the column other than free calcein. This might have resulted in possibly that the actual fraction of liposomes passed through the column either before or after the sample was collected.

Table 6 Phospholipid content in Mito-lipos

	Theoretic concentration [mM]	Actual concentration [mM]
Mito-lipo 1	0.5	0.5
Mito-lipo 2^-	0.3	0.0
Mito-lipo 4^+	0.3	0.2

The amounts of calcein encapsulated in various types of Mito-lipos are listed in Table 7. The amount of encapsulated calcein was found to be too small to be followed and provide any significant results during fusion experiment, therefor the calcein experiments were stopped at this point.

Table 7 Encapsulation efficiency of calcein

	Encapsulation efficiency (n = 3)	
	EE [%]	SD [%]
Mito-lipo 1	0.346	$3.5 \cdot 10^{-3}$
Mito-lipo 2^-	0.043	$8.8 \cdot 10^{-4}$
Mito-lipo 4^+	0.079	$2.3 \cdot 10^{-3}$

It has been stated that methods that base encapsulation on passive diffusion, like the film method used here, achieve small amounts of substances encapsulated (Zadi and Gregoriadis, 2000; Xu et al., 2012). As a result of steric hindrance, molecules with high molecular weight might therefore give low encapsulation efficiency (Adrian and Huang, 1979; Brandl, 2001). With Lipinski's "rule of 5" in mind (Lipinski et al., 1997), calcein has a relative high molecular weight and with the high number of hydrogen bond acceptors the hydrodynamic size of the molecule will increase thereby increasing the steric hindrance.

Another important fact that might affect the encapsulation process, and possibly also stability, is that after lipid film rehydration with IB-calcein, the presence of un-dissolved lipids was visible in the samples, floating on the surface. After extrusion, the suspensions were clear, but after storage precipitated lipids were observed again. This was not seen with the R18 mito-lipos, therefor it might be contributed to the effect of calcein. It has been shown that liposomes made of phospholipids can hydrolyse in aqueous medium resulting in free fatty acids and lyso-phospholipids which will affect the stability of the suspension (Grit and Crommelin, 1992). More experiments are needed to clarify this phenomenon, including methods to analyse the precipitates.

6 Conclusion

Up to date, there are no published data related the approach used in this project for mitochondrial targeting. To take advantage of the alternating fusion-fission cycle of mitochondria seems as an interesting way with potential in specific drug delivery and targeted distribution.

The prepared liposomes had a lipid composition similar to the composition of outer mitochondrial membrane and variations in the composition were made in order to optimize the fusion efficiency.

Particle size of the different preparations were controlled in the same range, and results of four months stability testing suggests that zeta potential did not affect stability of liposomes.

All liposomal suspensions were able to fuse but their efficiency varied. This indicates that some of the lipids play highly positive role in fusion process and other might have limiting role. These findings can be used in further optimization of liposomal formulation. We are hoping that in the near future more information will be available on such exciting new area of mitochondrial delivery.

7 Perspectives

Short term perspectives:

- Optimize lipid composition relative to fusion efficiency
- Increase encapsulation efficiency, for example by using a different and/or smaller fluorescent dye
- Compare uptake of hydrophilic substance via fusion and absorption from buffer to evaluate the efficiency of the delivery system

Long term perspectives:

- Evaluate intracellular movement in intact cells
- Evaluate stability by using relevant drug

8 References

Adrian, G. and Huang, L. (1979). Entrapment of proteins in phosphatidylcholine vesicles. *Biochemistry* **18**: 5610-5614.

AnaSpec (2009). Rhodamine 123. *Cerficate of Analysis*. California, USA.

Azad, M. B., Chen, Y. and Gibson, S. B. (2009). Regulation of autophagy by reactive oxygen species (ROS): implications for cancer progression and treatment. *Antioxid Redox Signal* **11**: 777-790.

Bahia, A. P., Azevedo, E. G., Ferreira, L. A. and Frezard, F. (2010). New insights into the mode of action of ultradeformable vesicles using calcein as hydrophilic fluorescent marker. *Eur J Pharm Sci* **39**: 90-96.

Bartlett, G. R. (1959). Phosphorus assay in column chromatography. *J Biol Chem* **234**: 466-468.

Becker, W. M., Kleinsmith, L. J. and Hardin, J. (2006a). Peroxisomes. *The World of the Cell*. 6th ed. San Francisco, California, Pearson Education: p. 356.

Becker, W. M., Kleinsmith, L. J. and Hardin, J. (2006b). The Tricarboxylic Acid Cycle: Oxidation in the Round. *The World of the Cell*. 6th ed. San Francisco, California, Pearson Education: p. 257.

Becker, W. M., Kleinsmith, L. J. and Hardin, J. (2006c). Cell Signals and Apoptosis. *The World of the Cell*. 6th ed. San Francisco, California, Pearson Education: p. 421.

Bio-Rad *DC Protein Assay Instruction Manual*. California, USA.

Biotium (2006). Octadecyl rhodamine B chloride (R18). *Product and safety data sheet*. California, USA.

Bitounis, D., Fanciullino, R., Iliadis, A. and Ciccolini, J. (2012). Optimizing Druggability through Liposomal Formulations: New Approaches to an Old Concept. *ISRN Pharm* **2012**: 11.

Boddapati, S. V., D'Souza, G. G., Erdogan, S., Torchilin, V. P. and Weissig, V. (2008). Organelle-targeted nanocarriers: specific delivery of liposomal ceramide to mitochondria enhances its cytotoxicity in vitro and in vivo. *Nano Lett* **8**: 2559-2563.

Brandl, M. (2001). Liposomes as drug carriers: a technological approach. *Biotechnol Annu Rev* **7**: 59-85.

Cali, T., Ottolini, D. and Brini, M. (2011). Mitochondria, calcium, and endoplasmic reticulum stress in Parkinson's disease. *Biofactors* **37**: 228-240.

Chen, L. B. (1989). Fluorescent labeling of mitochondria. *Methods Cell Biol* **29**: 103-123.

Chen, Y., McMillan-Ward, E., Kong, J., Israels, S. J. and Gibson, S. B. (2007). Mitochondrial electron-transport-chain inhibitors of complexes I and II induce autophagic cell death mediated by reactive oxygen species. *J Cell Sci* **120**: 4155-4166.

Churchward, M. A. and Coorssen, J. R. (2009). Cholesterol, regulated exocytosis and the physiological fusion machine. *Biochem J* **423**: 1-14.

Correia, S. C., Santos, R. X., Carvalho, C., Cardoso, S., Candeias, E., Santos, M. S., Oliveira, C. R. and Moreira, P. I. (2012). Insulin signaling, glucose metabolism and mitochondria: major players in Alzheimer's disease and diabetes interrelation. *Brain Res* **1441**: 64-78.

Daum, G. (1985). Lipids of mitochondria. *Biochim Biophys Acta* **822**: 1-42.

Desagher, S. and Martinou, J. C. (2000). Mitochondria as the central control point of apoptosis. *Trends Cell Biol* **10**: 369-377.

Ehehalt, R., Braun, A., Karner, M., Fullekrug, J. and Stremmel, W. (2010). Phosphatidylcholine as a constituent in the colonic mucosal barrier--physiological and clinical relevance. *Biochim Biophys Acta* **1801**: 983-993.

Enns, G. M. (2003). The contribution of mitochondria to common disorders. *Mol Genet Metab* **80**: 11-26.

Farooqui, A. A., Horrocks, L. A. and Farooqui, T. (2000). Glycerophospholipids in brain: their metabolism, incorporation into membranes, functions, and involvement in neurological disorders. *Chem Phys Lipids* **106**: 1-29.

Frezza, C., Cipolat, S. and Scorrano, L. (2007). Organelle isolation: functional mitochondria from mouse liver, muscle and cultured fibroblasts. *Nat Protoc* **2**: 287-295.

Gogvadze, V., Orrenius, S. and Zhivotovsky, B. (2009). Mitochondria as targets for cancer chemotherapy. *Semin Cancer Biol* **19**: 57-66.

Grit, M. and Crommelin, D. J. (1992). The effect of aging on the physical stability of liposome dispersions. *Chem Phys Lipids* **62**: 113-122.

Hoch, F. L. (1992). Cardiolipins and biomembrane function. *Biochim Biophys Acta* **1113**: 71-133.

Hoekstra, D., de Boer, T., Klappe, K. and Wilschut, J. (1984). Fluorescence method for measuring the kinetics of fusion between biological membranes. *Biochemistry* **23**: 5675-5681.

Hornig-Do, H. T., Gunther, G., Bust, M., Lehnartz, P., Bosio, A. and Wiesner, R. J. (2009). Isolation of functional pure mitochondria by superparamagnetic microbeads. *Anal Biochem* **389**: 1-5.

Houtkooper, R. H. and Vaz, F. M. (2008). Cardiolipin, the heart of mitochondrial metabolism. *Cell Mol Life Sci* **65**: 2493-2506.

Hu, Y., Moraes, C. T., Savaraj, N., Priebe, W. and Lampidis, T. J. (2000). Rho(0) tumor cells: a model for studying whether mitochondria are targets for rhodamine 123, doxorubicin, and other drugs. *Biochem Pharmacol* **60**: 1897-1905.

Huang, M., Camara, A. K., Stowe, D. F., Qi, F. and Beard, D. A. (2007). Mitochondrial inner membrane electrophysiology assessed by rhodamine-123 transport and fluorescence. *Ann Biomed Eng* **35**: 1276-1285.

Indran, I. R., Tufo, G., Pervaiz, S. and Brenner, C. (2011). Recent advances in apoptosis, mitochondria and drug resistance in cancer cells. *Biochim Biophys Acta* **1807**: 735-745.

Jianping, D. (2010). Mutation of mitochondria genome: trigger of somatic cell transforming to cancer cell. *Int Arch Med* **3**: 4.

Kaasalainen, M., Makila, E., Riikonen, J., Kovalainen, M., Jarvinen, K., Herzig, K. H., Lehto, V. P. and Salonen, J. (2012). Effect of isotonic solutions and peptide adsorption on zeta potential of porous silicon nanoparticle drug delivery formulations. *Int J Pharm* **431**: 230-236.

Kang, M. H. and Reynolds, C. P. (2009). Bcl-2 inhibitors: targeting mitochondrial apoptotic pathways in cancer therapy. *Clin Cancer Res* **15**: 1126-1132.

Kimball's Biology Pages online database. *Micrograph of mitochondria* [Cited 2012.05.06]; http://users.rcn.com/jkimball.ma.ultranet/BiologyPages/C/CellularRespiration.html.

Kowald, A. and Kirkwood, T. B. (2011a). Evolution of the mitochondrial fusion-fission cycle and its role in aging. *Proc Natl Acad Sci U S A* **108**: 10237-10242.

Kowald, A. and Kirkwood, T. B. (2011b). The evolution and role of mitochondrial fusion and fission in aging and disease. *Commun Integr Biol* **4**: 627-629.

Lasic, D. D. (1998). Novel applications of liposomes. *Trends Biotechnol* **16**: 307-321.

Lipinski, C. A., Lombardo, F., Dominy, B. W. and Feeney, P. J. (1997). Experimental and computational approaches to estimate solubility and permeability in drug discovery and development settings. *Adv Drug Deliv Rev* **23**: 3-25.

Marchi, S., Giorgi, C., Suski, J. M., Agnoletto, C., Bononi, A., Bonora, M., De Marchi, E., Missiroli, S., Patergnani, S., Poletti, F., Rimessi, A., Duszynski, J., Wieckowski, M. R. and Pinton, P. (2012). Mitochondria-ros crosstalk in the control of cell death and aging. *J Signal Transduct* **2012**: 17.

Marconescu, A. and Thorpe, P. E. (2008). Coincident exposure of phosphatidylethanolamine and anionic phospholipids on the surface of irradiated cells. *Biochim Biophys Acta* **1778**: 2217-2224.

Martin, A., Sinko, P. J. and Taylor, S. (2006). Biomaterials. *Martin's physical pharmacy and pharmaceutical sciences*. 5th ed. Philadelphia, Lippincott Williams & Wilkins: p. 618-620.

McMillin, J. B. and Dowhan, W. (2002). Cardiolipin and apoptosis. *Biochim Biophys Acta* **1585**: 97-107.

Molecular Expressions™ online database. *Structure of mitochondria* [Cited 2012.05.06]; http://micro.magnet.fsu.edu/cells/mitochondria/mitochondria.html.

Moreira, P. I., Carvalho, C., Zhu, X., Smith, M. A. and Perry, G. (2010). Mitochondrial dysfunction is a trigger of Alzheimer's disease pathophysiology. *Biochim Biophys Acta* **1802**: 2-10.

Mrsny, R. J., Volwerk, J. J. and Griffith, O. H. (1986). A simplified procedure for lipid phosphorus analysis shows that digestion rates vary with phospholipid structure. *Chem Phys Lipids* **39**: 185-191.

Naudi, A., Jove, M., Ayala, V., Cassanye, A., Serrano, J., Gonzalo, H., Boada, J., Prat, J., Portero-Otin, M. and Pamplona, R. (2012). Cellular dysfunction in diabetes as maladaptive response to mitochondrial oxidative stress. *Exp Diabetes Res* **2012**: 14.

Nelson, D. L. and Cox, M. M. (2008). Oxidation of Fatty Acids. *Lehninger Principles of Biochemistry*. 5th ed. New York, W. H. Freeman and Company: p. 653.

Nie, J., Hao, X., Chen, D., Han, X., Chang, Z. and Shi, Y. (2010). A novel function of the human CLS1 in phosphatidylglycerol synthesis and remodeling. *Biochim Biophys Acta* **1801**: 438-445.

Niebergall, L. J. and Vance, D. E. (2012). The ratio of phosphatidylcholine to phosphatidylethanolamine does not predict integrity of growing MT58 Chinese hamster ovary cells. *Biochim Biophys Acta* **1821**: 324-334.

Nunnari, J. and Suomalainen, A. (2012). Mitochondria: in sickness and in health. *Cell* **148**: 1145-1159.

O'Connor, J. E., Vargas, J. L., Kimler, B. F., Hernandez-Yago, J. and Grisolia, S. (1988). Use of rhodamine 123 to investigate alterations in mitochondrial activity in isolated mouse liver mitochondria. *Biochem Biophys Res Commun* **151**: 568-573.

Otera, H. and Mihara, K. (2012). Mitochondrial dynamics: functional link with apoptosis. *Int J Cell Biol* **2012**: 10.

Ow, Y. P., Green, D. R., Hao, Z. and Mak, T. W. (2008). Cytochrome c: functions beyond respiration. *Nat Rev Mol Cell Biol* **9**: 532-542.

Peng, A., Pisal, D. S., Doty, A. and Balu-Iyer, S. V. (2012). Phosphatidylinositol induces fluid phase formation and packing defects in phosphatidylcholine model membranes. *Chem Phys Lipids* **165**: 15-22.

Petruzzella, V., Sardanelli, A. M., Scacco, S., Panelli, D., Papa, F., Trentadue, R. and Papa, S. (2012). Dysfunction of mitochondrial respiratory chain complex I in neurological disorders: genetics and pathogenetic mechanisms. *Adv Exp Med Biol* **942**: 371-384.

Pieczenik, S. R. and Neustadt, J. (2007). Mitochondrial dysfunction and molecular pathways of disease. *Exp Mol Pathol* **83**: 84-92.

Reddy, P. H. (2008). Mitochondrial medicine for aging and neurodegenerative diseases. *Neuromolecular Med* **10**: 291-315.

Roerdink, F., Wassef, N. M., Richardson, E. C. and Alving, C. R. (1983). Effects of negatively charged lipids on phagocytosis of liposomes opsonized by complement. *Biochim Biophys Acta* **734**: 33-39.

Rolo, A. P. and Palmeira, C. M. (2006). Diabetes and mitochondrial function: role of hyperglycemia and oxidative stress. *Toxicol Appl Pharmacol* **212**: 167-178.

Roy, S. M., Bansode, A. S. and Sarkar, M. (2010). Effect of increase in orientational order of lipid chains and head group spacing on non steroidal anti-inflammatory drug induced membrane fusion. *Langmuir* **26**: 18967-18975.

Sato, M. and Sato, K. (2012). Maternal inheritance of mitochondrial DNA: Degradation of paternal mitochondria by allogeneic organelle autophagy, allophagy. *Autophagy* **8**: 424-425.

Scherer, M. and Schmitz, G. (2011). Metabolism, function and mass spectrometric analysis of bis(monoacylglycero)phosphate and cardiolipin. *Chem Phys Lipids* **164**: 556-562.

Schug, Z. T. and Gottlieb, E. (2009). Cardiolipin acts as a mitochondrial signalling platform to launch apoptosis. *Biochim Biophys Acta* **1788**: 2022-2031.

Sigma-Aldrich® online database. *Calcein* [Cited 2012.05.05]; http://www.sigmaaldrich.com/catalog/product/sigma/c0875?lang=en&region=NO.

Taylor, R. W. and Turnbull, D. M. (2005). Mitochondrial DNA mutations in human disease. *Nat Rev Genet* **6**: 389-402.

Torchilin, V. P. (2005). Recent advances with liposomes as pharmaceutical carriers. *Nat Rev Drug Discov* **4**: 145-160.

Torchilin, V. P. (2010). Passive and active drug targeting: drug delivery to tumors as an example. *Handb Exp Pharmacol* **197**: 3-53.

Torchilin, V. P. and Weissig, V. (2003). Preparation of Liposomes. *Liposomes : a practical approach*. 2nd ed. Oxford, Oxford University Press.

Trikash, I., Gumenyuk, V. and Lishko, V. (2010). The fusion of synaptic vesicle membranes studied by lipid mixing: the R18 fluorescence assay validity. *Chem Phys Lipids* **163**: 778-786.

Twig, G., Hyde, B. and Shirihai, O. S. (2008). Mitochondrial fusion, fission and autophagy as a quality control axis: the bioenergetic view. *Biochim Biophys Acta* **1777**: 1092-1097.

Wang, C. and Youle, R. J. (2009). The role of mitochondria in apoptosis*. *Annu Rev Genet* **43**: 95-118.

Wassef, N. M. and Alving, C. R. (1993). Complement-dependent phagocytosis of liposomes. *Chem Phys Lipids* **64**: 239-248.

Weiss, H., Friedrich, T., Hofhaus, G. and Preis, D. (1991). The respiratory-chain NADH dehydrogenase (complex I) of mitochondria. *Eur J Biochem* **197**: 563-576.

Weissig, V. (2011). Mitochondrial delivery of biologically active molecules. *Pharm Res* **28**: 2633-2638.

Welti, R. and Glaser, M. (1994). Lipid domains in model and biological membranes. *Chem Phys Lipids* **73**: 121-137.

Westermann, B. (2010). Mitochondrial fusion and fission in cell life and death. *Nat Rev Mol Cell Biol* **11**: 872-884.

Xu, X., Khan, M. A. and Burgess, D. J. (2012). Predicting hydrophilic drug encapsulation inside unilamellar liposomes. *Int J Pharm* **423**: 410-418.

Zadi, B. and Gregoriadis, G. (2000). A Novel Method for High-Yield Entrapment of Solutes into Small Liposomes. *J Liposome Res* **10**: 73-80.

Zanatta, C. F., Sato, A. M., Camargo Junior, F. B., Campos, P. M. and Rocha-Filho, P. A. (2010). Rheological behavior, zeta potential, and accelerated stability tests of Buriti oil (*Mauritia flexuosa*) emulsions containing lyotropic liquid crystals. *Drug Dev Ind Pharm* **36**: 93-101.

Zhang, Y. and Chan, D. C. (2007). New insights into mitochondrial fusion. *FEBS Lett* **581**: 2168-2173.

Zhou, Y. (2012). Mito-liposomes: A potential delivery strategy for mitochondrial targeting via membrane fusion activity. *PhD Thesis;* Albert-Ludwigs-Universität Freiburg, Freiburg im Breisgau, Germany.

Zick, M., Rabl, R. and Reichert, A. S. (2009). Cristae formation-linking ultrastructure and function of mitochondria. *Biochim Biophys Acta* **1793**: 5-19.

Zungu, M., Schisler, J. and Willis, M. S. (2011). All the little pieces. -Regulation of mitochondrial fusion and fission by ubiquitin and small ubiquitin-like modifer and their potential relevance in the heart. *Circ J* **75**: 2513-2521.